# INITIAL PERFORMANCE STUDY OF THE UTIAS HIGH ENERGY MOLECULAR BEAM FACILITY

by

D. R. O'Keefe



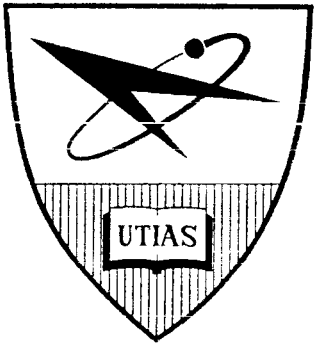


AUGUST 1964

UTIAS TECHNICAL NOTE NO. 75

# INITIAL PERFORMANCE STUDY OF THE UTIAS HIGH ENERGY MOLECULAR BEAM FACILITY

by

D. R. O'Keefe

AUGUST, 1964

UTIAS TECHNICAL NOTE NO. 75

## ACKNOWLEDGEMENT

The author wishes to thank Professor J.B. French for the assistance and advice given throughout this research endeavour as well as R.E. Stokes for his contributions to both the design and construction of the apparatus. Advice given by J.H. Davis, Jr. is also greatly appreciated.

This work was performed under the National Aeronautics and Space Administration Grant No. NSG 367, under the technical cognizance of Dr. A. Gessow, Chief, Physics of Fluids Program. Financial assistance both from this source and the Defense Research Board of Canada is gratefully acknowledged.

## SUMMARY

12411

Initial performance studies have been carried out on the U. T. I. A. S. high energy molecular beam facility. A mixture of 99.0 mole percent helium and 1 mole percent argon was expanded through an orifice into a high vacuum region. A conical sharp-edged skimmer was placed on the centre line of the expanding flow. A movable source made it possible to vary the source-skimmer distance and investigate the effect of this variable on the flux and spatial distribution of the beam in a collimation chamber downstream. In all cases, the resulting beam was found to be enriched in the heavier species (argon). Collisions between the light and heavy particles will tend to yield a beam in argon which has a directed velocity approaching that of the helium. Some of the parameters influencing the increase in the mole fraction of argon have been investigated. For the experimental conditions used, results suggest that free molecular flow of both gases through the skimmer entrance is the condition for this enrichment to be a maximum. The radial distribution of the beam at a fixed position downstream of the skimmer was obtained using an omegatron mass spectrometer as a detector connected to a traversing impact probe. The addition of helium to a pure argon flow was shown to have a marked collimation effect on the argon. The molar fluxes on the center line of the beam in the collimation chamber for a 139 torr and room temperature source were found to be 90.4 mole percent helium and 9.6 mole percent argon. At the same position downstream of the skimmer (46 inches), the centre line beam fluxes were $5 \times 10^{13}$ and $4.7 \times 10^{14}$ molecules/cm$^2$ sec for the argon and helium respectively. An attempt has been made to correlate the Mach numbers obtained from an analysis of the radial distribution of the molecular fluxes of each species with the flow Mach numbers which might be expected in the free jet expansion.

TABLE OF CONTENTS

## LIST OF SYMBOLS

| | |
|---|---|
| $A$ | area of flow from supersonic nozzle at skimmer station |
| $a$ | radius of collimator (probe) orifice |
| $A_1$ | area of skimmer orifice |
| $A_*$ | throat area of supersonic nozzle |
| $a_o$ | sound speed in the source |
| $C_{m_1}$ | most probable random speed in the region of the skimmer |
| $d_o$ | diameter of nozzle (source orifice) |
| $d_1$ | diameter of skimmer orifice |
| $h$ | radial distance off axis at a station "L" downstream of the skimmer |
| $I_B$ | omegatron electron beam current |
| $K_{n_o}$ | Knudsen number referred to source orifice diameter |
| $K_{n_1}$ | Knudsen number referred to skimmer orifice diameter |
| $L$ | distance between skimmer and collimator or probe |
| $M_1$ | Mach number at skimmer entrance |
| $n$ | molecular density (molecules/$cm^3$) |
| $n_o$ | molecular density in the source |
| $N_{coll}$ | molecular flux (molecules/$cm^2$sec) at a collimator or probe placed on the centre line of the beam downstream of the skimmer. |
| $N_h$ | flux of molecules hitting a probe at a radial distance "h" off axis and at a fixed distance "L" downstream of skimmer |
| $P_o$ | stagnation pressure in the source |
| $P_a$ | ambient pressure in initial pumping stage |
| $Q_1$ | molecular flow (molecules/sec) through skimmer |

| | |
|---|---|
| $Q_*$ | molecular flow at throat of supersonic nozzle |
| $Q_\theta$ | molecular flow across the plane subtended by the cone of half angle $\theta$ |
| $S_1$ | $= U_1/C_{m_1}$ speed ratio of the flow at the skimmer |
| $T_1$ | temperature of the flow at the skimmer entrance |
| $U_1$ | bulk or particle velocity of the gas at the skimmer entrance |
| x | distance between source exit and skimmer entrance |
| $\Lambda$ | omegatron peak height (amps) |
| $\chi$ | omegatron peak height above background (amps) |
| $\gamma$ | ratio of specific heats |
| $\lambda_{1_L}$ | Lagrangian mean free path at skimmer entrance |
| $\lambda_{1_E}$ | Eulerian mean free path calculated from $\lambda_{1_L}$ and $M_1$ |
| $\xi$ | $= \frac{L^3}{(h^2 + L^2)^{\frac{1}{2}}} \cdot N_h$ in molecules/sec |
| $\sigma'$ | enrichment factor based on total flow of heavier species through the skimmer $\sigma' = \frac{\alpha + 1}{\alpha' + 1}$ |
| $\sigma''$ | enrichment factor based on the flux of the heavier species as measured at the collimator (probe) downstream of the skimmer and on the centre line of the beam $\sigma'' = \frac{\alpha + 1}{\alpha'' + 1}$ |
| $\alpha$ | ratio of the mole fraction of helium to argon in the source |
| $\alpha'$ | ratio of the overall flow of helium to argon into the collimation chamber after the skimming process |
| $\alpha''$ | ratio of the flux of helium to argon as seen in the collimation chamber by a collimator (probe) placed in the centre line of the beam |

Subscripts

| | |
|---|---|
| 1 | refers to skimmer station |
| o | refers to source conditions |
| * | refers to sonic (throat) conditions |

## 1. INTRODUCTION

Attempts to produce high energy (1 - 10ev) molecular and atomic beams have been initiated by the desire of investigators to study both gas-surface and gas-gas interactions in this energy range. This range is intermediate between the low energy capabilities of the classical oven beam and the much higher energies attainable with present-day ion beam systems.

To an aerodynamicist, a facility capable of producing such an energetic molecular beam will permit serious studies of the type of gas-surface interactions experienced by a satellite in orbit about the earth. An accurate measure of both the normal and tangential accommodation coefficients for various surfaces, will serve to predict the drag forces on a satellite and may eventually lead to a design which will enable them to remain in orbit longer.

The molecules and atoms of primary interest in such investigations are those typically experienced by a satellite at an altitude of between one hundred and five hundred miles; they are nitrogen, oxygen, hydrogen and helium. Initially it is proposed that studies be performed using the inert gases, since in doing so, the added complications of chemisorption at the surface are eliminated. The term "molecule" will be used throughout this report to describe any particle being accelerated in the beam system.

The use of the skimmed exhaust from a supersonic nozzle for the production of intense molecular beams with narrow energy spread was first proposed by Kantrowitz and Grey (Ref. 1). A beam obtained in this manner from a heated source at 2000°K will yield particle velocities for the light gases (helium and hydrogen) in the satellite range (10 km/sec). To obtain beams of the same velocity for the heavier (nitrogen, oxygen, argon) gases, it has been proposed by Becker, Bier and Burghoff (Ref. 2) that a seeding technique be used.

A brief description of this seeding technique is as follows. The initial mixture of seed (heavy species) gas and carrier (light species) gas is allowed to expand in a free jet into a region of low pressure. The core of the jet is then extracted by a conical skimmer placed several nozzle diameters downstream of the throat. The beam is collimated at a position further downstream and then used for the surface studies. It is found that the collimated beam contains more of the heavier species than does the initial mixture. This enrichment is believed to be due to several factors; these include pressure diffusion in the initial expansion, possible collisional effects in the transition portion of the flow either before or after the skimming and differences in the mean thermal velocities of the different species in the free molecular beam. The net result will be a beam enriched in the heavier gas at a particle velocity approaching that of the lighter species.

Energy augmentation for a beam from a given source temperature will depend on how low the mean molecular weight of the mixture can be made. For this reason, a relatively small amount of seed gas is used compared to the large amount of carrier gas.

The facility at U. T. I. A. S. has been designed for source pressures and temperatures up to 1 atmosphere and 2500°K respectively, although all of the work reported here is for the 139 torr and 300°K source conditions.

## 2. DESCRIPTION OF EXPERIMENTAL APPARATUS

### 2.1 Description of Molecular Beam Facility

A schematic view of the facility is provided in Fig. 2.1-a, illustrating the three sections of primary interest. Figure 2.1-b is a photograph of the facility as it appears at present. A detailed description of the various components of the beam system will now be presented.

#### 2.1.1 Source Chamber and Gas Introduction System

The oven source is located in the pumping manifold of the U. T. I. A. S. low density wind tunnel. A very complete description of this facility is given by Enkenhus (Ref. 3). It suffices to say here that its nine Edwards model 18B3 oil booster diffusion pumps represent a pumping capacity of about 11,000 litres/sec for air. They are backed by two Kinney Model DVD-141418 mechanical pumps placed in parallel. Pressure in the tunnel, for the .031" diameter nozzle with source stagnation pressure and temperature of 139 torr and 300°K respectively, does not exceed 25 microns. The source itself consists of a stainless steel tube of 1/8" inside diameter with a .031" hole drilled in the side of it. It is positioned in relation to the skimmer by a traversing mechanism of three degrees of translational freedom and one of rotation. Flexible steel cables placed through the vacuum wall provide the driving mechanism. The oven carriage has been designed to allow for a linear expansion along the length of the tube. This will be necessary when heated sources are used. Tungsten-rhenium tubes will be used and a D.C. electrical power supply has been installed to ohmically heat the source to temperatures approaching 2500°K.

Gas from commercial supply bottles is introduced into the oven source through a flow metering system. Control is accomplished by means of two Edwards type LB. 2A needle valves. Pressures upstream of these are slightly above atmospheric, preventing the leakage of any impurities in from the outside. Flows are measured using Fischer and Porter Tri-flat variable area flow meters. Downstream of the needle valves and flow meters, the two gases (argon-helium) are mixed and passed through a liquid nitrogen trap for purification and then into the oven tube. Stagnation pressures are measured with a Wallace and Tiernan type FA-160 gauge.

### 2.1.2 Skimmer

Sharp-edged skimmers for the cold source ($T_o$ = 300°K) beam have been made from brass and stainless steel. Skimmers with orifice diameters as small as .014" have been handworked under the microscope. All the cones have had external and internal half angles of 35 and 25 degrees respectively.

Success in making a tungsten skimmer for heated beams has been realized. Tungsten sprayed brass cones have been drilled and then etched to give an extremely sharp edge. The ratio of the radius of the skimmer edge to that of the hole size has been estimated to be smaller than 0.01.

### 2.1.3 Collimation Chamber

The collimation chamber provides a region in which the separation process in the mixed beam may continue after the skimming process (if densities remain high enough),and as well, provides ample room for instrumentation with which to study the resulting molecular fluxes and velocity distributions. Attenuation by collisions with the background molecules is reduced to a negligible level by using an NRC model HS 32-32,000 fractionating oil diffusion pump. This attains a pressure level typically of $10^{-6}$torr. Heater operation at 16 KW with Narcoil-40 oil, gives (for air) a pumping speed greater than 30,000 1/sec in the range of $10^{-5}$ to 6 x $10^{-4}$ torr. The pump is operated untrapped so as to retain the maximum pumping speed available. It was proposed that instead of using two such pumps with traps, that an untrapped pump be used with a small trapping section added downstream to prevent the migration of oil molecules into the experimental test section (see Fig. 2.1-a). The same two Kinney type DVD-141418 mechanical pumps, as described above, are used for backing. At blank off, a pressure of 2 x $10^{-6}$ torr is readily obtainable and is the ultimate expected with the type of oil used. The pressure in the chamber is measured with a Consolidated Vacuum Corporation type GP4-100A cold cathode discharge gauge.

### 2.1.4 Trapping Section

The trapping section consists of a cannister about 3 inches in diameter and 6 inches long. It is completely fabricated from stainless steel parts with heliarc welded joints. A concentric cylinder of copper screening holds a charge of molecular seive material(Linde type 13x). The charge may be added through a conflat (double knife edge flanges with a soft copper gasket between) sealed port on the side. A valve in this section is also available for pumping down when outgassing of the material is desired. The entire assembly is bakeable to aid in the outgassing process. The end plates are used to position two small stainless steel tubes (.040 inches in diameter) which provide the final collimation of the beam. Flexible bellows on either side of the cannister, as well as a spherically

seated joint on one of the end plates allow for an accurate alignment with the skimmer orifice. Motions are imparted in the vertical and horizontal directions by micrometers. A 3 inch diameter gate valve between collimation and trapping sections can be used to isolate one system from the other.

### 2.1.5 Experimental Test Section

Since the emphasis in the gas-surface interaction studies to be conducted is on ultra clean conditions, the experimental test section must be completely bakeable and capable of pressures in the ultra high vacuum range. A bakeable experimental chamber employing a 500 litre/sec getter-ion pump is under construction, which should attain vacua better than $10^{-9}$ torr under the gas load imposed by the beam. Pressures of this order are desirable in any serious studies to be made, since about twenty minutes are required for mono-layer formation after target cleaning. There is also an advantage in beam detection since the ratio of beam signal to background noise is increased with lower background pressure. The fact that the experimental test chamber is completely separate from the remainder of the apparatus, allows different experiments to be prepared concurrently in separate exchangeable test chambers.

## 2.2 Omegatron Measuring System

### 2.2.1 Gauge Volume

Incorporated in the collimation chamber is a pressure measuring probe system which may be operated either as an impact pressure measuring device or used to obtain the background pressure. These pressures are measured with an omegatron and a Bayard-Alpert ionization gauge. Figure 2.1-a indicates the location of the gauge system. The portion of the gauge volume containing the above pressure measuring devices is outside the collimation chamber and is isolated from the oil vapour by a liquid nitrogen trap. Pressures measured with the Bayard-Alpert gauge are then due to those gases not removed by the trap, often called noncondensables. The background pressure of noncondensables in the collimation chamber is typically $3 \times 10^{-7}$ torr.

The gauge volume itself is made entirely from heliarc welded stainless steel. Valve "A" is an Edwards 1 inch diameter diaphragm type valve. It serves to isolate the entire gauge volume, including trap, from the collimation chamber. Valve "B", a one inch type L Granville-Phillips bakeable ultra high vacuum valve, serves to isolate the important gauge components from the trap. Conflat flanges secure the gauge components to the system. Glass-to-kovar seals are used on the glass components.

The entire system outside the collimation chamber can be baked to 450°C with a portable oven. Valve "A" is protected with water cooling coils. Extended bakes at 300°C with heater tapes have been found adequate when the system is being prepared for operation. When the trap becomes sufficiently contaminated, valve "B" is closed and the trap baked until the contaminants have been driven back into the collimation chamber. Liquid nitrogen is then replaced and clean operation for an extended period of time is again realized. The magnet for the omegatron is mounted on a positioner and can be moved out of the way during the bakeout cycle.

The Bayard-Alpert gauge electrodes are outgassed by ohmic heating. The omegatron has been outgassed by RF induction heating to 800°C, but this procedure was not necessary for the present application where two gases (argon and helium) widely spaced in the spectrum are being considered.

A Balzers IMG-U1 controller is used to operate the IM-8 Bayard-Alpert gauge. A current reading is obtained from this controller which had been calibrated for operation with air so that a direct reading in torr is available. Calibration of the upper ranges against a Mc Leod gauge has shown this direct reading to be quite accurate. When gases other than air are being considered, it becomes necessary to multiply the reading on the controller by a conversion factor which is the ratio of the ionization cross section of the gas to be measured to that of the effective cross section of air. Conversion factors provided by the manufacturer have been found accurate. The gauge was found to be very useful both as a continuous monitor of total pressure changes in the system and as a calibrated instrument when only one gas was being used.

The signal current from the omegatron was amplified by a Keithley 603 electrometer amplifier. Since the mass spectrum is scanned by varying the frequency of the RF voltage applied to the omegatron, a motorized drive on the RF oscillator coupled with a strip chart recorder on the output of the electrometer, allows a convenient recording of mass spectra.

### 2.2.2 Probe Head Assembly

A photograph of the traversing probe assembly is shown in Fig. 2.2-b. A flexible copper hose 3-1/2 feet long and 1 inch inside diameter connects the main probe body with the gauge volume. The probe itself is at a fixed distance (46 ± 1/4 inches) downstream of the skimmer orifice, but can be moved vertically and horizontally. The horizontal traverse has a maximum displacement of 2 inches and is used merely to find the centre of the beam. The vertical traverse, on the other hand, has a displacement across the entire collimation chamber. This degree of freedom allows one to obtain the radial distribution of flux for the individual gases once they have passed through the skimmer. The probe body itself is provided with a motor driven face plate. A thin walled orifice, 0.120

inches in diameter, is present in the plate. In the opened position, a so called "flag" prevents the beam molecules from passing directly into the orifice and so a background pressure reading is obtained. In the closed position, on the other hand, the orifice sees the beam molecules plus background. A simple subtraction then yields the flux of the beam molecules which is incident on the probe. The radial distribution of the beam molecules is then easily obtained. This simple subtraction technique was found to be quite adequate for the present measurements, but future measurements of the velocity distributions involve such a reduction in beam signal that a double omegatron system is being constructed. In such a case, the background signal will be electrically subtracted, resulting in a large increase in signal-to-noise ratio.

## 3. EXPERIMENTAL RESULTS

### 3.1 Source Mass Flow Calibration

The Fischer and Porter Tri-flat variable area flow meters were calibrated for argon and helium using the water displacement technique at atmospheric pressure. Flows were measured directly in atmospheric cc/sec and results are included in Figs. 3.1-a and 3.1-b. Employing the equation for the flow of gas through a supersonic nozzle (Ref. 8, page 139), a calculation was performed and compared with the experimentally measured flow. Correlation was within one percent, suggesting that the geometrical diameter of the source was a true measure of the throat diameter of the jet. Consequently, all calculations have been performed employing this geometrical dimension. The present arrangement allows for oven mixtures in the range .002 to .15 mole fraction of argon in helium.

### 3.2 Collimation Chamber Mass Flow Calibration

The HS 32-32,000 diffusion pump has a different pumping speed for argon than for helium. As well, the gases have different ionization cross sections and this had to be taken into account when omegatron readings were interpreted. A separate calibration for the collimation chamber was then required for determining the flux through the skimmer in normal operation. To remain within the operating pressure of the omegatron ($< 10^{-5}$ torr), it was necessary to calibrate very small flows (2.0 to $10^{-2}$ atm cc/sec). These were measured by timing the advance of a soap bubble between two points on a calibrated scale. These flows were then admitted to the collimation chamber directly and peak height measurements made with the omegatron, thus relating peak heights to known flows for each species. Figure 3.2-a is a peak height versus flow calibration for argon and Fig. 3.2-b is for helium. From these calibration curves the actual amount of either gas passing through the skimmer can then be obtained. This yields an enrichment factor for the total gas flow passing through the skimmer. This may not necessarily be the actual enrichment factor for the stream tube which impinges on the skimmer opening, since the

skimmer itself may influence the flow in front of it appreciably. The large scatter in results for helium at high flow values is due to the error in timing the advance of the soap bubble.

### 3.3 Operating Characteristics of the Omegatron

Curves of the variation of the omegatron peak height with molecular density for both argon and helium are illustrated in Figs. 3.3-a, 3.3-b, 3.3-c and 3.3-d. For the argon there is no significant departure from linearity until a pressure of about $5 \times 10^{-5}$ torr is reached. Helium, on the other hand, displays a rather abrupt change at about $10^{-5}$ torr. It is believed that this fall-off of current at high pressures is due to a combination of two effects, the presence of non-resonant ions, and the collisions of the ions with neutral molecules as these ions spiral out to the collector. For more detail, the reader is referred to one of the original papers on omegatron operation (Refs. 4 and 5). The recommended operating region for the omegatron is then below $10^{-5}$ torr.

The above curves have been found to be very dependent on the potentials assigned to the omegatron electrodes. Figure 3.3-e is a schematic representation of the omegatron electrode system and will aid the reader in the discussion to follow. Even for argon, departures from linearity at relatively low pressures have been found to occur when optimization of the peak height was not complete. Optimization was carried out by varying the electrode potentials until a maximum output current for the omegatron was obtained. Trap and RF bias voltages have been found to require almost the same setting for either the argon or helium optimization.

The electron collector potential is a relatively unimportant factor. By far the most controlling of all parameters has been found to be the electron beam current,which is a function of the filament heater voltage for a constant filament bias. Figures 3.3-f and 3.3-g show how the electron beam current affects the peak heights of the argon and helium. All other potentials are maintained at the predetermined optimum values. To obtain these curves, the filament bias was maintained at -90 volts and the heater voltage varied to obtain the electron beam current. The omegatron peak heights for argon and helium are maximum at 1.4 and 0.85 microamps respectively. It is suggested that the decrease in ion collection current at large electron beam currents is due to the formation of a large number of non-resonant ions in the ionizing region. These appreciably disturb the electric field lines, resulting in a smaller number of resonant ions being collected.

Above 1 microamp of electron beam current, the effect discussed above causes one gas species to be affected by the presence of the other. Helium peak heights were decreased by as much as 20% upon the introduction of argon. This effect vanished entirely for currents less than 0.6 microamps; consequently all measurements were taken at 0.5 micro-

amp operation. Argon did not display any changes when helium was added, even at 1 microamp operation. This may be explained by the fact that the axial drift velocity of the helium ions due to their own space charge is higher than that for argon, so that helium ions are much less effective in changing the collection of argon ions than vice versa.

The RF Voltage was found to influence strongly the shape of the argon peak. This control was varied until a symmetric peak resulted over all pressure ranges. Peak heights were then used as an indication of the amount of the species present; an integrated curve was not used.

The omegatron optimization is found to be dependent on the value of the resistance between ion collector and ground. This resistance causes a change in the potential on the ion collector and makes it necessary to readjust trap and bias voltages. This was done each time the resistance in the Keithley 603 preamplifier was changed.

The best operating characteristics of the omegatron (Electron Technology Inc.) have been found at the following settings:

filament bias voltage = -90 volts
electron collector voltage = +18 volts
trap voltage = +1.0 volts
RF voltage = 7.6 volts peak to peak at 1 mcs.

The RF bias control setting, which aids in preventing non-resonant ions from reaching the collector, was also optimized.

### 3.4 Flow in Front of the Skimmer

Photographs of the flow have been taken employing a glow discharge technique. Figure 3.4-b shows one such photograph taken with a nozzle pressure ratio "$P_o/P_a$" of $4 \times 10^3$. Love et al (Ref. 6) have calculated the location of the Mach disc for the free jet expansion of a diatomic gas at relatively small values of $P_o/P_a$. Figure 3.4-a is such an expansion showing the formation of a Mach disc ($P_o/P_a = 33.2$)*. Rothe (Ref. 7) has extended this work to that of a monatomic gas. An extrapolation of this data up to large values of the pressure ratio, such as encountered in this work, yields the formation of a Mach disc which is extremely far out from the source. In the present situation, the shock should appear at a nozzle-skimmer distance ($x/d_o$) of 266. The physical implausibility of such a statement is made manifest when one realizes that on the basis of Woolf's (Ref. 9) extension of the Owen and Thornhill

---

* Due to Rothe

(Ref. 10) curve (Fig. 3.4-c) this distance corresponds to an extremely large Mach number ($M > 100$). Such a large value is not expected, since at some position in the expansion, the collision frequency will become sufficiently low that no further increase in Mach number can occur. In fact, the concept of a Mach number becomes meaningless. Beyond this point, the jet becomes a purely radially expanding flow of the type suggested by Fig. 3.4-b.

A measurement has been made of the total flow of each species coming through the skimmer. With the face of the impact probe opened, and the beam "flagged", background pressures in the collimation chamber are obtained. The conversion from peak height, as measured by the omegatron, to flows, is then accomplished through the use of Figs. 3.2-a and 3.2-b. The flow of the gases from the 99% - 1% source mixture is shown as a function of nozzle-skimmer distance in Fig. 3.4-d. A theorectical prediction of this flow can be made assuming isentropic conditions.

The molecular flow at the throat of a supersonic nozzle is given by (Ref. 8)

$$Q_* = \left(\frac{2}{\gamma+1}\right)^{\frac{\gamma+1}{2(\gamma-1)}} \cdot n_o\, a_o\, A_* \text{ (molecules/sec)} \qquad (3.4.1)$$

Assuming a one dimensional expansion to a Mach number of $M_1$ at the skimmer entrance, the total flow through the skimmer is given by

$$Q_1 = \frac{A_1}{A} \cdot Q_* = \frac{A_1}{A_*} \cdot \frac{A_*}{A} \cdot Q_* \qquad (3.4.2)$$

where "A" represents the area of the flow at the skimmer position and "$A_1$" is the skimmer area. "$A_*$" and "$Q_*$" are the area and flow respectively of the throat section.

Employing the well-known gas dynamic relation for the ratio $A_*/A$ one obtains

$$Q_1 = A_1\, n_o\, a_o\, M_1 \left(1 + \frac{\gamma-1}{2} \cdot M_1^2\right)^{-\left[\frac{\gamma+1}{2(\gamma-1)}\right]} \qquad (3.4.3)$$

For helium gas at 298°K and at a stagnation pressure of 134 torr, as used in the present work, the relevant quantities are:

$$n_o = 4.34 \times 10^{18} \text{ molecules/cm}^3$$
$$a_o = 1.013 \times 10^5 \text{ cm/sec}$$
$$A_1 = 1.05 \times 10^{-3} \text{ cm}^2$$
$$\gamma = 1.67$$

from which

$$Q_1 = 4.62 \times 10^{20}\, M_1 \left(1 + 0.335\, M_1^2\right)^{-1.99} \text{(molecules/sec)} \qquad (3.4.4)$$

Using Fig. 3.4-c, the theoretical flow can then be calculated for the various $x/d_o$ values. Figure 3.4-d includes this theoretical prediction. This curve is seen to approach the experimental one at values of $x/d_o$ greater than 20. The disagreement at the smaller values is believed due to the presence of a very diffuse shock in front of the skimmer which prevents it from accepting all of the molecules in the stream tube defined by the skimmer orifice. A Knudsen number calculation, based on the skimmer orifice diameter, is found to exceed 10 for $x/d_o$ values of 22.0 or greater, and it is in this region that the theoretical and experimental curves are seen to come into reasonable agreement. Mean free paths have been calculated from room temperature viscosity data based on the hard sphere model of interaction. The inadequacy of such a calculation is discussed in section 3.6. It is not possible with the present probe system to obtain skimmer flows for $x/d_o$ values greater than 25, since it then becomes extremely difficult to distinguish the beam signal from the background noise. Large scatter is present in the results beyond the $x/d_o$ values of 15, because of this effect.

## 3.5 Enrichment in the Expansion Process

The experimental helium and argon flow curves found in Fig. 3.4-d can be used directly to compute the enrichment in the flow at the skimmer entrance. An enrichment factor $\mathcal{G}'$ is defined as the ratio of the mole percentage of argon measured in the final flow to that of the original mixture. If $\alpha$ represents the ratio of the amount of helium to argon in the source mixture ( $\alpha = 99$ for a 99% - 1% helium-argon mixture) and $\alpha'$ is the ratio of the amount of helium to argon passing through the skimmer, then $\mathcal{G}' = (\alpha + 1)/(\alpha' + 1)$ .

Figure 3.6-c illustrates the behaviour of the enrichment over the $x/d_o$ range considered. It displays an increase from 2.2 to 4.4 over this range, with most of the change occurring in the vicinity of an $x/d_o$ of 14.0. Although enrichments were not obtained for $x/d_o > 25.0$, it appears that $\mathcal{G}'$ is maximum in the situation where the skimming takes place after collisions in the flow have ceased.

Several authors have investigated the enrichment of a gas mixture expanded in a free jet. The source mixtures used by Reis and Fenn (Ref. 11) have a larger mole fraction of the heavier species than the work reported here. Using a skimmer type probe, their measurements show the variation of enrichment with nozzle-skimmer distance, and indicate a pronounced maximum. The nozzle-skimmer distance at which this maximum appears is dependent on the source pressure. This maximum appears at nozzle-skimmer distances ($x/d_o$ values) of approximately 10 and 6 for source pressures of 200 and 50 torr respectively. In the present work (Fig. 3.6-c), enrichment is not found to decrease in value even up to as high as 25.0 nozzle diameters. Measurements beyond this point were experimentally impractical because the beam signal became indistinguishable from fluctuations in the background noise at $x/d_o$ values greater than 25.0. The

best enrichment reported by Reis (Ref. 11) (using the notation of this report) is $\mathcal{G}' = 2.5$ for a 50 torr source mixture composed of 80% hydrogen and 20% nitrogen.

Becker, Bier and Burghoff (Ref. 2) have also reported enrichments in the heavier component gas along the centre line of the flow. Employing a 97.8% hydrogen and 2.2% argon mixture at a 15 torr source pressure, they have found an increase in enrichment up to nozzle-skimmer distances of six. Results were not obtained for larger $x/d_o$ values.

Chow (Ref. 12) has reported an enrichment in oxygen for the flow of air from a supersonic nozzle. The enrichment on the centre line was found to increase with distance from the nozzle exit. However, enrichments were found to be present across the entire flow field, making the techniques used in these investigations doubtful (Ref. 13).

3.6 The Enrichment Along the Centre Line

The molecular flux on the centre line of the beam has been measured with the stagnation-static probe assembly. These flux measurements are obtained by subtracting the omegatron peak height readings for operation in the opened and closed modes as described in section 2.2.2. Respective number densities are found from Figs. 3.3-a and 3.3-c. The assumption of room temperature conditions in the gauge volume, determines the average velocity "$\bar{c}$". The flux from this volume is then calculated for the equilibrium situation (the flux into the gauge is equivalent to the flux out) by the simple kinetic theory expression "$1/4\ n\bar{c}$". The orifice of the probe is a 0.120 inch diameter hole in a 0.001 inch thick tungsten foil.

With the stagnation-static probe assembly at a fixed distance (46 inches) downstream of the skimmer orifice, the molecular flux at the centre line was measured as a function of nozzle-skimmer distance. The experimental curves in Fig. 3.6-a display the same general form for both the argon and the helium. At distances close to the skimmer, the relatively small value of the flux is attributed to a detached shock behind which the flow deflects, so that some of the stream tube defined by the skimmer hole is spilled. The gradual increase with nozzle-skimmer distance is a result of the change towards a shock-free condition.

Kantrowitz and Grey (Ref. 1) and later Parker et al (Ref. 14) have developed an expression for the beam flux through a second collimator downstream of the skimmer. The impact probe orifice is actually this second collimator in the present situation.

With the assumption that there are no collisions after the skimmer entrance and that continuum conditions exist upstream, then the theoretical flux is

$$N_{coll} = \left[ \frac{A_1 n_o a_o M_1}{\left\{1 + \frac{1}{2}(\gamma - 1) M_1^2\right\}^{\frac{\gamma+1}{2(\gamma-1)}}} \right] \cdot (3 + \gamma M_1^2) \cdot \left( \frac{1}{2\pi L^2} \right) \qquad (3.6.1)$$

Where $A_1$ is area of skimmer orifice ($1.05 \times 10^{-3}$ cm$^2$)

$M_1$ is Mach number at skimmer entrance

$\gamma$ is ratio of specific heats (1.67)

L is the distance between the skimmer entrance and the collimator. ($117.0 \pm 0.5$ cm)

$n_o$ is the density in the source ($4.34 \times 10^{18}$ molecules/cm$^3$)

$a_o$ is the sound speed in the source ($1.013 \times 10^5$ cm/sec)

The flux predicted by equation 3.6.1 is included in Fig. 3.6-b where the experimental values obtained are also plotted. Experimental points are found to lie considerably below the theoretical prediction. This general behaviour has also been found by Deckers and Fenn (Ref. 15). They have described the tendency for agreement at the high $x/d_o$ values as being due both to the approach to free molecular conditions downstream of the skimmer, and to the disappearance at large nozzle-skimmer separations of skimmer interference such as diffuse shock waves or viscous effects. For distances close to the source, this will no longer be true and a large departure from the predictions of equation 3.6.1 is expected.

The enrichment along the centre line of the beam in the collimation chamber can now be computed from the curves of Fig. 3.6-a. By definition, $\mathcal{G}'' = (\alpha + 1)/(\alpha'' + 1)$ where again $\alpha$ is the ratio of the amount of helium to argon in the source, but now $\alpha''$ is the ratio of helium to argon flux as seen by a collimator on the centre line of the beam downstream of the skimmer. Results are included in Fig. 3.6-c over the complete range of nozzle-skimmer distances studied. An increase for larger $x/d_o$ values is quite evident with the appearance of a sudden change at $x/d_o = 8.0$. A comparison of $\mathcal{G}''$ and $\mathcal{G}'$ at the larger nozzle-skimmer distances is in order here. For $x/d_o = 24.0$, $\mathcal{G}'' = 2.16\,\mathcal{G}'$, indicating that there is a relative increase of the argon flux on the centre line downstream of the skimmer. More will be said about this collimation effect in section 3.8.

It has been reported by Klingelhöfer and Lohse (Ref. 16) that a source mixture of 99% hydrogen and 1% argon has lead to a beam composed of 60% hydrogen and 40% argon at a collimator downstream. In the present beam generation studies, a 90.4% helium - 9.6% argon beam has been measured at the collimator for the 99% helium - 1% argon source mixture. It is believed that larger source stagnation pressures will lead to a better collimation effect (section 3.8) and hence to a better enrichment. In the present system, it was not possible to exceed one atmosphere in the source. This limitation is not due to any failure of the first pumping stage in handling the gas load, but is rather a gas feed problem. A modification will be made shortly allowing a more direct comparison with the results of reference 13, where stagnation pressures of 3.05 atmospheres have been employed.

Use of a coordinate system moving with the bulk motion of the gas will lead to a prediction of the Lagrangian mean free path in front of the skimmer. At the various nozzle-skimmer distances, Mach numbers are obtained from Fig. 3.4-c, and conventional gasdynamic isentropic flow tables used to predict the density. The arbitrary choice of a hard sphere interaction model between particles then allows one to calculate the Lagrangian mean free path ( $\lambda_{1_L}$ ) for the density obtained. These " $\lambda_{1_L}$" values are plotted in Fig. 3.6-d. The corresponding Knudsen number values, based on the skimmer diameter, are presented in Fig. 3.6-e. It is interesting to note that the so called transition region ($1 \leq Kn_1 \leq 10$) appears between nozzle-skimmer distances of 7.2 and 22.4 respectively. This is also the region over which molecular fluxes and enrichment factors undergo their largest variation. The shortcomings of such a calculation are referred to by Reis and Fenn (Ref. 11). They refer to the uncertainty in such calculations as being due to the extremely low temperature of the flow at the high Mach numbers concerned. At such low temperatures, the viscosity-derived collision cross sections based on room temperature conditions cease to be reliable. The above authors have made estimates of mean free paths based on low temperature viscosity data and have found appreciable disagreement with higher temperature calculations.

With the present probe system, it was not possible to obtain a continuous measurement of nozzle-skimmer distances greater than 28.0. It was purely a mechanical design limitation which made these relatively large values difficult to measure. A reading was taken at an $x/d_o = 60.7$ and the resultant enrichment factor ( $\mathcal{G}''$ ) was found to have the value 8.2. The decrease is believed due to the scattering of the beam molecules by the background gas between nozzle and skimmer. The helium and argon fluxes at this particular station were $3.59 \times 10^{14}$ and $3.2 \times 10^{13}$ molecules/$cm^2$ sec respectively. Both values are a decrease over the values found at the higher $x/d_o$ values of Fig. 3.6-a.

## 3.7 The Radial Distribution of the Gas Species in the Region Downstream of the Skimmer

A study was made of the radial spatial distribution of the beam flux in both argon and helium by traversing radially across the beam with the probe. Fluxes were measured by the same method as described in section 2.2.2. Two distributions were taken at two different nozzle-skimmer distances. The distribution in figure 3.7-a was taken in the region where $\mathcal{G}''$ has been shown to level out at presumably its maximum value ($x/d_o = 24.2$). The width at one half maximum is 1.4 inches for the argon and 3.05 inches for the helium. The reader will notice immediately that the argon distribution does not fall to zero at large radial distances. An attempt will be made later to account for this observation.

A distribution (Fig. 3.7-b) was also taken at a nozzle-skimmer distance of 9.07, a value at which the greatest changes in $\mathcal{G}''$ are

being experienced. The flux is less as predicted by the data of Fig. 3.6-a. Also the distributions become much wider, having a width at half maximum of 3.15 inches for argon and one which is considerably larger for the helium. It is also apparent that both the argon and helium distributions do not fall to zero at the large radial distances off axis. The implications of such a result will be discussion in section 3.8.

These distributions have been plotted in terms of the peak height above background "$\chi$" but conversion to flux in molecules/$cm^2$sec can be made through use of the expressions included in the figure. The term "peak height above background" refers to the difference between the peak height as measured by the omegatron probe system in the "unflagged" mode and that measured as background when operated in the "flagged" mode.

## 3.8 Collimation Effect of the Heavier Species when Mixed with the Lighter One

The effect of the helium carrier on the radial distribution of argon emanating from the skimmer was observed by comparing the radial distribution of the same argon flow (0.5 atm cc/sec) both alone and in a 99% helium - 1% argon source mixture. Figure 3.7-a demonstrates the resulting collimation in the argon due to the presence of the lighter species. The flux of argon on the centre line increases from $2.22 \times 10^{13}$ to $5.2 \times 10^{13}$ molecules/$cm^2$sec upon the addition of the helium. As well, the width at one half maximum decreases from 2.65 to 1.4 inches. The latter value represents an angular spread of 1.7 degrees measured at the skimmer orifice. The above behaviour is qualitatively predicted if it is assumed that, in the initial expansion stage, the argon suffers enough collisions with the helium to have its particle velocity raised to a value approaching that of the latter. In such a case, the random radial components of the argon velocity will be less effective in making the gas come off axis, with a much narrower distribution resulting.

A numerical integration of the flux distributions of figures 3.7-a and 3.7-b should yield the total flow of the gas coming through the skimmer. When this integration is performed for the helium distribution of figure 3.7-a, a flow is calculated which is 25 percent of that measured experimentally for the total flow through the skimmer (Fig. 3.4-d). A possible explanation is the presence of uniform scattering in the region in front of the skimmer, of the type suggested by Fenn (Ref. 17). Helium atoms will suffer as many collisions into the skimmer orifice as into the region external to it, with no net change in the total flow into the collimation chamber. However, the molecules scattered into the skimmer will be in the form of a very broad beam and there is evidence that with the present single omegatron detection system such a signal will not be distinquishable from the background. An estimate of the error in reading signals close to background can account for the discrepancy, if the "missing" helium atoms are distributed over a large enough area in the

in the collimation chamber. This explanation could account for the contradiction between the good agreement with theory in Fig. 3.4-d and the apparent discrepancy in Fig. 3.7-a.

In the argon curves of Figs. 3.7-a and 3.7-b, a measurable $\chi$ value ($\simeq 0.5 \times 10^{-12}$ amps) is obtained for radial distances greater than 2.0 inches. It is suggested that this measurable flux is a scattered beam and that the peaked distribution is a separate unscattered addition to it. A numerical integration of the flux under the peaked distribution (Fig. 3.7-a) yields the same value of the flow for both the mixed and pure argon case. These values, however, are 6 and 30 percent respectively of the experimentally determined values of the flow through the skimmer. This suggests that the so called "missing" argon atoms are contained in the scattered beam and that there is a higher proportion scattered when helium is added to the flow. In the pure argon case, the air and argon background in front of the skimmer may account for the scatter, while in the mixed case, the helium as well has an effect. Purely effusive flow of the argon background gas through the skimmer does not account for the large amount contained in this broad beam.

It is interesting to note that a numerical integration of the flux for the argon distribution (mixed flow) of figure 3.7-b yields the same value for the molecular flow as the two argon distributions of figure 3.7-a. This calculated flow is 4 percent of the skimmer flow measured experimentally in figure 3.4-d ($x/d_o = 9.07$). Therefore, an even larger percentage of the argon appears in the scattered beam for smaller nozzle-skimmer distances, as might be expected.

These explanations must be regarded as conjecture only, because of the lack of systematic data to corroborate them. At present, a much more sensitive double omegatron system is being installed together with an axial velocity analyser. It is hoped that a systematic investigation using these techniques can answer the many questions which remain concerning the expansion and beam formation processes.

## 3.9 Analysis of Flux Distribution from Skimmer

A theoretical prediction of the distribution of the gas species at a fixed distance downstream of the skimmer can be obtained by assuming that the molecules which pass through the skimmer have a Maxwellian velocity distribution function with a superimposed uniform bulk velocity (so called "drifting Maxwellian velocity distribution"). However, as already stated in section 3.4 and qualitatively supported by Fig. 3.4-b, there should exist, sufficiently far out from the source, a region where the flow becomes collisionless and purely effusive (surface AB in Fig. 3.7-c). Beyond this point, there will be no further change in the speed ratio, since in the absence of collisions, neither the most probable random velocity (temperature) nor the particle velocity is changed. If the skimmer

is placed in this collisionless region, and should it be possible to predict the speed ratio (Mach number) from studies made in the collimation chamber, then it will be possible to find the $x/d_o$ value at which collisions cease. The isentropic Mach number prediction will then be employed only up to this $x/d_o$ value. Such a speed ratio determination can be made from the form of the beam fluxes in the collimation chamber, if an axially parallel rather than radially expanding bulk velocity is assumed.

Since the solid angle subtended by the skimmer from the probe measuring position is small, the assumption of a point source at the skimmer entrance will be made. If the expansion were complete and all of the random components removed from the flow at this point, all of the molecules would fall on the centre line and there would essentially be only the very small skimmer width to the distribution downstream. These random components will cause the gas to come off axis, being vectorially added to the bulk velocity of the flow at the point of skimming.

The Maxwellian velocity distribution in cylindrical coordinates and in the drifting frame of reference can be written as

$$f = \frac{n_1}{(\sqrt{\pi}\, C_{m_1})^3} \cdot e^{-\frac{(V_r^2 + V_z^2)}{C_{m_1}^2}} \qquad (3.9.1)$$

where

$n_1$ is the molecular density at the skimmer

$C_{m_1}$ is the most probable random velocity in the region at the skimmer entrance $C_{m_1} = (2\,kT_1/m)^{\frac{1}{2}}$

$T_1$ is the temperature at the skimmer

$V_r$, $V_z$ are the components of the random velocity in the radial and axial directions as shown in Fig. 3.9-a

Denoting the bulk velocity at the skimmer entrance by $U_1$, the following expression for the flow (molecules/sec) across the plane subtended by the cone of half angle $\theta$ is obtained

$$Q_\theta = \frac{n_1 A_1}{(\sqrt{\pi}\, C_{m_1})^3} \int_0^{(U_1+V_z)\tan\theta} \int_{-U_1}^{\infty} \int_0^{2\pi} (V_z + U_1) V_r\, e^{-\frac{(V_r^2+V_z^2)}{C_{m_1}^2}}\, d\phi\, dV_z dV_r \qquad (3.9.2)$$

where the cylindrical volume element in velocity space is $V_r dV_r d\phi dV_z$.

Following the suggestion of Kantrowitz and Grey (Ref. 1), for large Mach numbers, the random velocity component "$V_z$" is neglected with respect to "$U_1$". Also, the lower limit on "$V_z$" is approximated by $-\infty$. The upper limit on "$V_r$", the radial random velocity component, arises from the fact that from a point source at $z = 0$ only those $V_r$'s which are of magnitude less than that specified by $h/L = V_r/U_1 + V_z = \tan\theta$

will fall within the detection region at L. In the above expression, "L" is the distance of the measuring plane downstream of the skimmer and h is the radial position off axis.

So allowing $-U_1 = -\infty$ and $U_1 >> V_z$, equation 3.9.2 becomes

$$Q_\theta = \frac{2\pi n_1 A_1 U_1}{(\sqrt{\pi} C_{m_1})^3} \int_0^{U_1 \tan\theta} \int_{-\infty}^{\infty} V_r \, e^{\frac{-(V_r^2 + V_z^2)}{C_{m_1}^2}} dV_r dV_z \qquad (3.9.3)$$

which upon integration and substitution of the speed ratio ($S_1 = U_1/C_{m_1}$) yields

$$Q_\theta = U_1 \, n_1 \, A_1 \, (1 - e^{-S_1^2 \tan^2\theta}) \qquad (3.9.4)$$

This then gives the number of molecules per unit time crossing the plane at z = L and falling within the cone of half angle θ. To correlate this with what has been done experimentally, it is necessary to find the flux of molecules as measured by a probe a distance "h" off axis and at a distance "L" downstream.

The number of molecules/sec passing through a ring $\Delta\theta$ wide at the radial distance h off axis and at a distance L downstream of the skimmer is (see figure 3.9-b)

$$\frac{d\,Q_\theta}{d\theta} \cdot \Delta\theta \qquad (3.9.5)$$

For small angles "θ" and a probe orifice of radius "a"

$$\Delta\theta = \frac{2a}{P} = \frac{2a}{(h^2 + L^2)^{\frac{1}{2}}} \qquad (3.9.6)$$

Equation 3.9.4. is differentiated and multiplied by $\Delta\theta$ and the area weighting factor "$\pi a^2/4\pi a h$". From pure geometrical considerations, $\tan\theta = h/L$ and $\sec^2\theta = (h^2 + L^2)/L^2$ are also substituted resulting in a flux at the probe given by

$$N_h = \frac{U_1 \, n_1 \, A_1 \, S_1^2}{\pi} \left[\frac{(h^2 + L^2)^{\frac{1}{2}}}{L^3}\right] e^{-\left(\frac{S_1 h}{L}\right)^2} \qquad (3.9.7)$$

If the natural logarithm of both sides of Eq. 3.9.7 is taken, then the resulting equation is

$$\ln\left[\frac{L^3}{(h^2 + L^2)^{\frac{1}{2}}} \cdot N_h\right] = \ln\left[\frac{U_1 \, n_1 \, A_1 \, S_1^2}{\pi}\right] - \frac{S_1^2 \, h^2}{L^2} \qquad (3.9.8)$$

Thus a plot of the quantity $\xi = L^3/(h^2 + L^2)^{\frac{1}{2}} \cdot N_h$ vs $h^2/L^2$ on a semi-logarithmic scale should be linear if the assumptions used in the analysis are correct. In such a case the speed ratio $S_1$ can be determined directly from the slope.

A calculated Mach number can then be obtained from the relation $S = \sqrt{\gamma/2}\, M$, although the term Mach number is a meaningless concept in a collisionless flow since sound cannot be propogated. The only advantage in converting to Mach number is in attempting to relate this distribution of molecules back to the plane in the expansion up to which collisions have occurred and at which the concept of Mach number still has meaning. Peak heights above background ($\alpha$) were read directly from the figure and conversion to flux ($N_h$) made, employing the equations provided. Figure 3.9.-c shows the behaviour of "$\xi$" for the three distributions given in Fig. 3.7-a. The fluxes ($N_h$ values) for the argon curves of Fig. 3.9-c have been calculated from a new base line, determined from Fig. 3.7-a, and equivalent to $0.5 \times 10^{-12}$ amps. As explained previously in section 3.8, the larger values of "$\alpha$" off-axis are believed to be due to scattering, and consequently the fluxes ($N_h$) for the argon are obtained by subtracting the reading $0.5 \times 10^{-12}$ amps from the $\alpha$ values and then proceeding in the normal fashion as described above. The effect of this alteration on the linearity and slope of the curve was small.

Calculations were made to determine the behaviour of the quantity "$\xi$" for the distributions of Fig. 3.7-b. The broadness of these distributions compared to those of Fig. 3.7-a may be due to self-scattering in the beam downstream of the skimmer, and is considered a result of the higher beam densities which exist at smaller nozzle-skimmer separations. It was found that a non-linear variation of "$\xi$" with $(h/L)^2$ resulted in such a case.

The variation of "$\xi$" for the helium from the 99% - 1% source mixture ($x/d_o = 24.2$) is linear over most of the range and shows only a slight curvature for the higher $(h/L)^2$ values. A Mach number obtained from the slope of this curve has the value 28.8. The argon "$\xi$" variation has been included for completeness. It shows a departure from linearity for values of $(h/L)^2$ greater than $60 \times 10^{-5}$ and the Mach number calculated for this linear region is 37.4.

Before attempting any comparisons of the above results with isentropic predictions, one particular aspect of the above theoretical analysis should be considered. A skimmer looking into the flow at a distance far enough downstream to put it in the collisionless region will see the hypothetical surface AB (actually a region) at which collisions effectively cease. This surface will represent the origin of an infinite number of non-isotropic point sources as schematically represented in Figs. 3.9-d and 3.9-e. Consider first the ideal situation assumed in the above theoretical analysis. A plane AB (Fig. 3.9-d) is considered to exist upstream of the

skimmer. Consequently, all flux distributions on this plane will have their axes parallel to one another. A point P on axis will see the maximum of the distribution at r but a point P' off axis will see the side of the distribution located at r'. This will mean a decrease of the flux at the station z = L downstream, when moving outwards from P to P'. The distribution resulting is predicted by the analysis above.

In the actual situation, however, the surface at which these sources are located is curved (see Fig. 3.9-c), i.e. the flow is radially expanding. Since the distribution at r' is now inclined from the axis rP, the point P' sees a smaller flux than in the ideal situation. The result is a distribution at z = L which falls off more rapidly. In the plot of $\ln \mathcal{F}$ vs $(h/L)^2$, this will mean a more rapid radial decrease of the former, since $\mathcal{F}$ is proportional to $N_h$ (the flux at a distance h off axis). Since the slope gives the speed ratio (Mach number), then the net result is an apparent Mach number larger than that actually existing at the plane at which the collisions cease. The effect is most severe for expansions to high Mach numbers, since then the flux distribution will be extremely narrow and the angle of inclination of the distribution to rP most controlling. The effect is even greater as the skimmer is moved further downstream, since in such a case, the point P will be looking at a distribution further displaced from rP along the curve AB and further inclined to the axis. The qualitative arguments, as presented above, are supported by the data obtained from Fig. 3.9-c. The Mach number for helium was calculated to be 28.8 and shows close agreement with Woolf's (Fig. 3.4-c) isentropic prediction of 27.3. This seems to suggest that the skimmer is located at a point close to the region or plane in the expansion at which collisions cease ($x/d_o$ = 24.2). Although the helium considered here was mixed with argon in the amount 99% - 1%, the effect of the argon is completely neglected and the flow treated as if it were pure helium. The source stagnation pressure for helium was 134 torr, and assuming isentropic expansion to a Mach number of 27.3 (the theoretical value), one can calculate the temperature of the flow to be 1.19°K.

Arbitrarily choosing the hard sphere model of radius 1.09 Å, corresponding to room temperature viscosity data, the Lagrangian mean free path can be immediately obtained from Fig. 3.6-d. The result is a mean free path of 0.42 cm for the flow at the position where the Mach number was 27.3 and $x/d_o$ = 24.2. The corresponding Eulerian mean free path (referred to the laboratory coordinate system) can be obtained from the equation

$$\lambda_{1E} = \lambda_{1L} \cdot \frac{U_{1He}}{C_{1He}} = \sqrt{\frac{\gamma \pi}{8}} \cdot \lambda_{1L} \cdot M_1 \qquad (3.9.9)$$

where

$\lambda_{1E}$ is the Eulerian mean free path at the skimmer

$\lambda_{1L}$ is the Lagrangian mean free path at the skimmer

$U_{1_{He}}$ is the particle velocity for the helium at the skimmer

$\overline{C_{1_{He}}}$ is the mean random velocity of the helium at the skimmer

$\gamma$ is the ratio of specific heats

$M_1$ is the isentropic Mach number at the skimmer

Employing Eq. 3.9.9, the Eulerian mean free path for the helium ($x/d_o$ = 24.2) is found to be 10.6 cm. This represents a small collision frequency in itself, and if the density of the beam is considered to decrease as the square of the distance from the skimmer (a realistic assumption), then one can conclude that helium-helium collisions are negligible between skimmer and collimator.

Using the same approach as above, the respective mean free paths for argon-argon collisions in the mixed flow at the same nozzle-skimmer distance are $\lambda_{1L}$ = 9.9 cm and $\lambda_{1E}$ = 300 cm, suggesting that argon-argon collisions are not a consideration in the present system.

All beam analyses to date, including the one reported in this section, have assumed free molecular flow conditions downstream of the skimmer. It would appear, from the narrowness of the measured radial flux distribution taken at $x/d_o$ = 24.2, that collisions downstream of the skimmer are unimportant, as suggested by the arbitrarily calculated free paths, and that the effective increase in collision radius of the molecules at the very low temperatures has not had an important effect on the final beam.

The Mach number for the pure argon flow, obtained from Fig. 3.9-c, is larger than the value of 27.3 predicted by figure 3.4-c. The value of 37.4 can be qualitatively accounted for by the arguments presented above. Since the source stagnation pressure for the argon is only 5 torr, then the collisionless region appears much further upstream than for the helium. The apparent Mach number then should be larger than the isentropic prediction since the distribution at z = L is affected more by the curvature of the collisionless surface.

The calculated Mach number of the argon in the argon-helium mixture is 62.5. In this situation, the argon cannot be considered as a singly expanding species. Collisions with the much more abundant helium will have the effect of increasing the argon bulk velocity toward the value consistent with the mean molecular weight of the mixture, as discussed in section 3.8. It is interesting to perform the following calculation. In the absence of slip between the argon and helium gases, the argon should

attain the same temperature and particle velocity as the helium at the skimmer entrance. The isentropic Mach number (M = 27.3) at the $x/d_o$ value 24.2 is then used with the temperature (1.19°K) at this point to calculate the bulk velocity of the mixture, treating it as pure helium since the effect of the 1 mole % argon is small. With the assumption of expansion to the same temperature and same bulk velocity, it is then possible to calculate the Mach number of the argon in the mixture. Such a calculation yields a Mach number of magnitude 86.7. This is greater than the value of 62.5 calculated from the experimental results. One possible explanation is that the assumption of "no slip" is not a valid one and that the argon does fall behind the helium in the expansion. However, it is felt that all these Mach numbers are unrealistically high because of the radial expansion of the free molecular flow discussed earlier. The above discussion is qualitative only and merely suggestive of what might be occurring in the flow upstream of the skimmer.

## 4. CONCLUSIONS

An enrichment of the heavier species in binary gas mixtures on the centre line of the flow upstream of the skimmer has been described by Becker et al (Ref. 2) and Reiss and Fenn (Ref. 11). Such an enrichment has been found in the present studies. The total amount of argon passing through the skimmer represents a four fold increase over that present in the source mixture (99 mole % helium, 1 mole % argon).

An increase in flux of the argon on the centre line of the beam has been found when helium is added to the flow. Collisions between the light and heavy species in the initial stages of expansion are believed to be the cause of this collimation effect.

With the completion of the present study, it is now apparent that the seeding technique of Ref. 2 is practical for the generation of a high energy beam in argon. Indications are that a high Mach number flow has been achieved leading to a higher bulk velocity of the argon. As well, the flux of the argon ($5 \times 10^{13}$ molecules/$cm^2$sec) was high enough to allow simple differential detection techniques to be employed.

An undesirable aspect of the present results was the relatively impure beam that was obtained. The helium beam flux on the centre line was still about ten times that of the argon. At the expense of increased argon in the source mixture with the attendant drop in final attainable velocity, this separation could be improved upon considerably. However, the fact that slip may be present between the gases may make it possible to discriminate against the helium through the use of a rotating velocity selector. Also, it is believed that studies at much higher source pressures and temperatures should lead to better enrichments.

## REFERENCES


1. Kantrowitz, A. Grey, J. — Rev. Sci. Inst. 22, 328 (1951).

2. Becker, E. W. Bier, K. Burghoff, H. — F. Naturforsch 10a, 565 (1955).

3. Enkenhus, K. R. — The Design, Operation and Instrumentation of the U. T. I. A. Low Density Wind Tunnel, U. T. I. A. Report No. 44, June 1957.

4. Klopfer, A. — Das Omegatron als Partialdruckmesser, Allgemeine, Deutsche Philips Industrie G. m. b. H. Vortag Nr. 57. (1960).

5. Schuchhardt, G. — Ion Movements in an Omegatron, Vacuum Vol. 10, No. 5, pp. 373-376. (1960).

6. Love, E. S. Grigsby, C. E. Lee, L. P. Woodling, M. J. — Experimental and Theoretical Studies of Axisymmetric Free Jets, NASA T. R. R-6 (1959).

7. Rothe, D. — (private communication)

8. Leipmann, H. W. Roshko, A — Elements of Gasdynamics, John Wiley and Sons Inc., New York. (1960).

9. Sherman, F. S. — Self Similar Development of Inviscid Hypersonic Free Jet Flow, May 1963. Lockheed Report 6-90-63-61 (Contains calculations by Woolf on extension of Owen and Thornhill curve to larger distances downstream of nozzle exit for $\gamma$ = 5/3, 7/5 and 9/5 gases.)

10. Owen, P. L. Thornhill, M. A. — (1948) Aeronautical Research Council Reports and Memorandum 2616.

11. Reiss, V. Fenn, J. B. — Jour. of Chemical Physics, Vol. 39, No. 12 (1963).

12. Chow, R. R. — On the Separation Phenomena of Binary Gas Mixtures in an Axisymmetric Jet, University of California, Institute of Engineering Research HE-150-175 (1959).

13. Masson, B.S. — Diffusive Separation of a Gas Mixture Approaching a Sampling Probe, University of California, Institute of Engineering Research HE-150-206 (1962).

14. Parker, H.M. Kuhlthau, A.R. Zapata, R.N. Scott, J.E. Jr. — Rarefied Gasdynamics (Pergamon Press Inc., New York, 1960), pp. 69-79.

15. Deckers, J. Fenn, J.B. — Review of Scientific Instruments, Vol. 34 No. 1, 1963, pp. 96-100.

16. Klingelhöfer, R Lohse, P. — Reported at Conference on Molecular and Atomic Gas Beams and Related Problems 13-14 May 1963. University of Virginia (to be published in Physics of Fluids).

17. Fenn, J.B. Anderson, J.B. Andres, R.P. Maise, G. — Studies of Low Density Supersonic Jets, In the Proceedings of the Fourth International Symposium on Rarified Gas Dynamics at Toronto, Canada 1964 (Academic Press Inc.) (to be published).

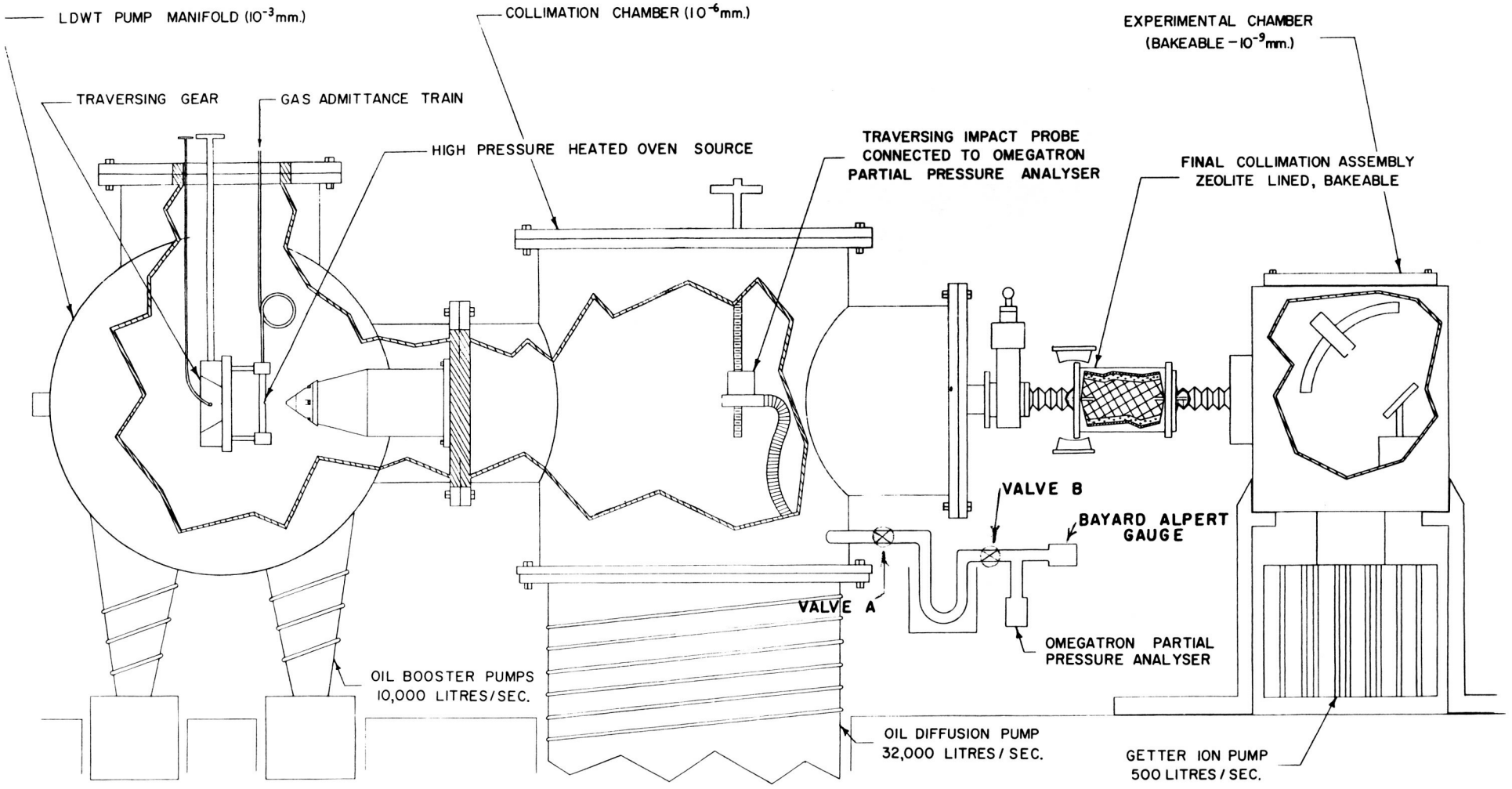


UTIA HIGH ENERGY MOLECULAR BEAM FACILITY

**FIGURE 2.1- a**

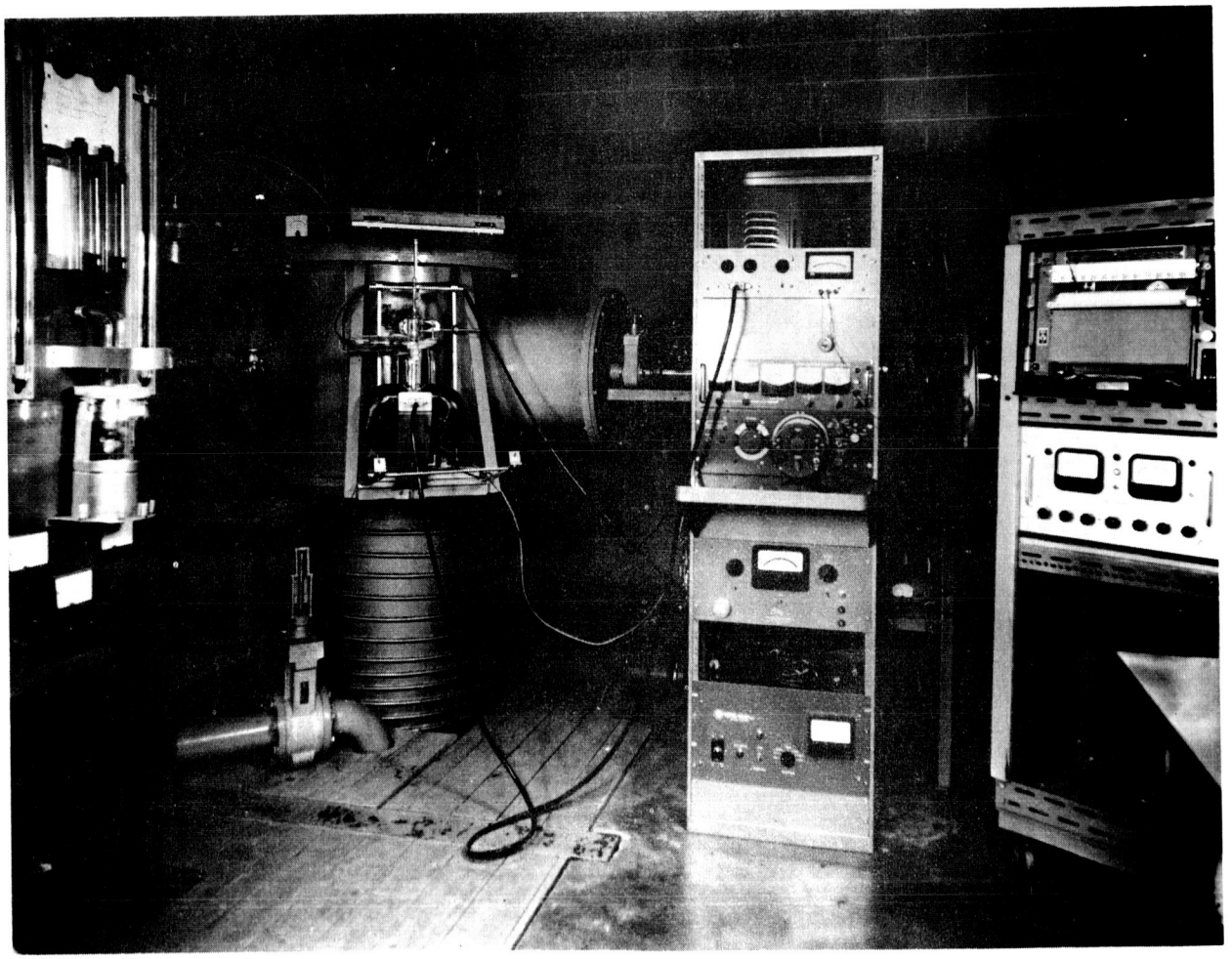

FIGURE 2.1- b MOLECULAR BEAM FACILITY

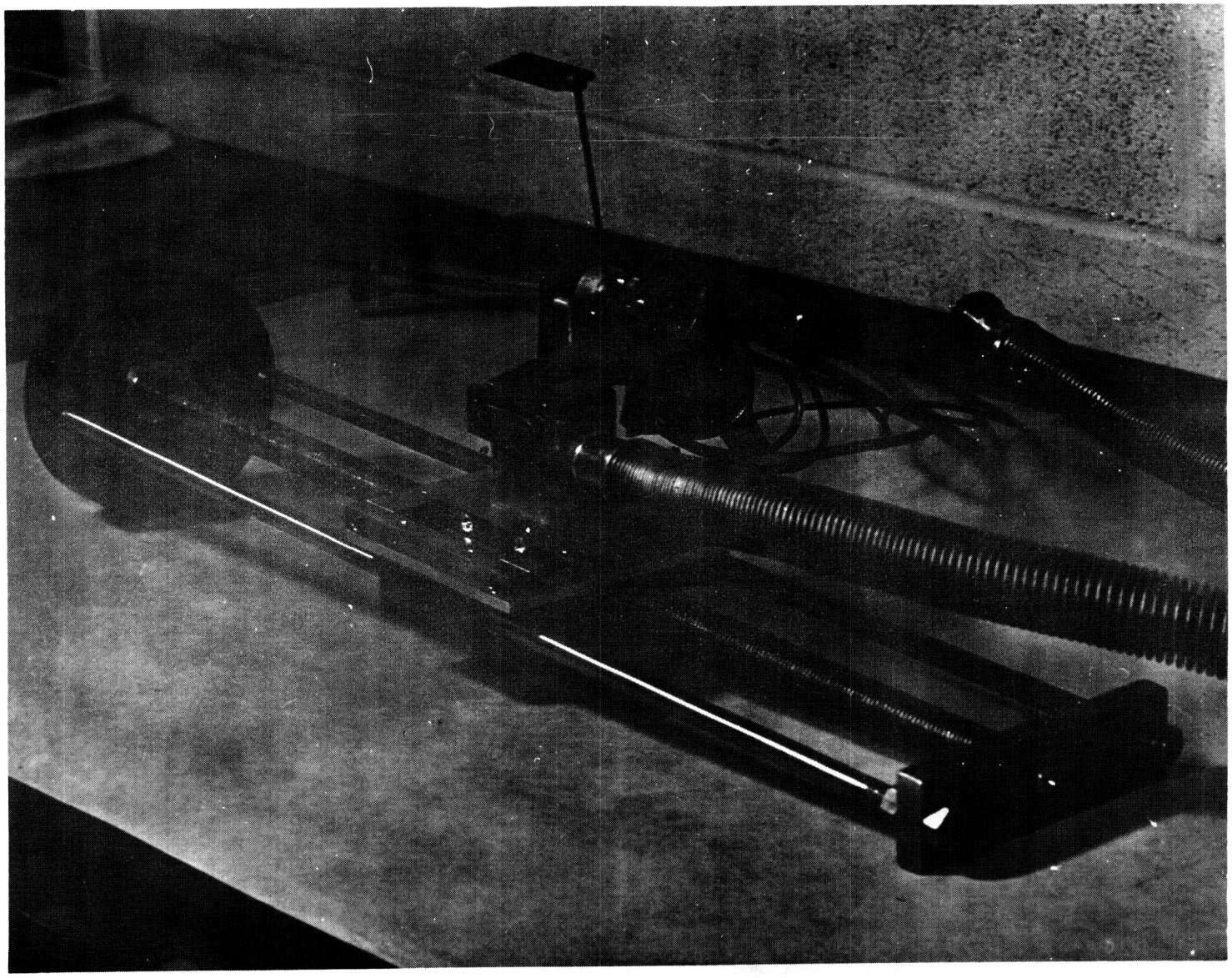

FIGURE 2.2- b PROBE HEAD ASSEMBLY

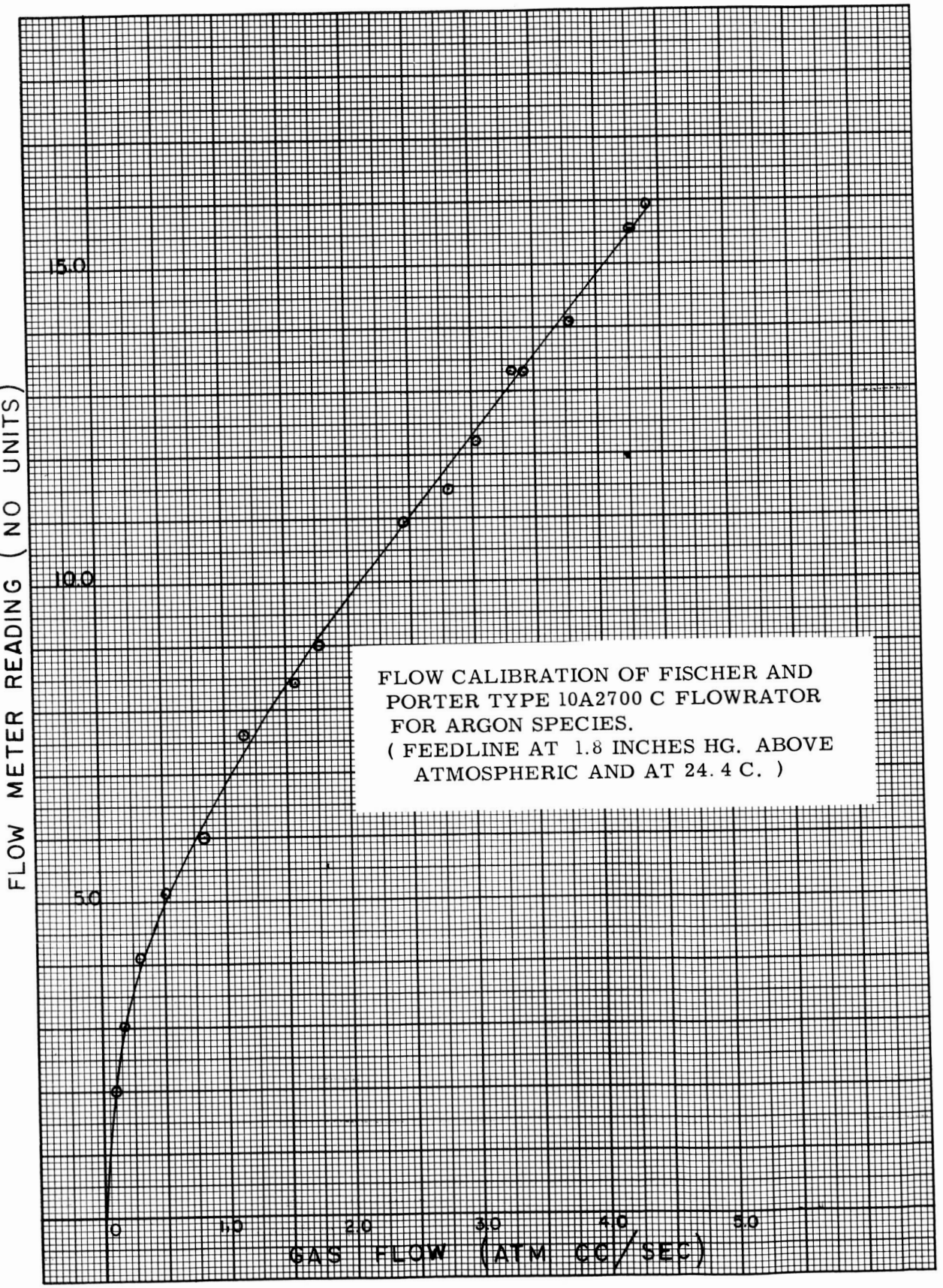
FLOW METER READING ( NO UNITS)
15.0
10.0
5.0
0
1.0
2.0
3.0
4.0
5.0
GAS FLOW (ATM CC/ SEC)
FLOW CALIBRATION OF FISCHER AND PORTER TYPE 10A2700 C FLOWRATOR FOR ARGON SPECIES.
( FEEDLINE AT 1.8 INCHES HG. ABOVE ATMOSPHERIC AND AT 24.4 C. )

FIGURE 3.1-a

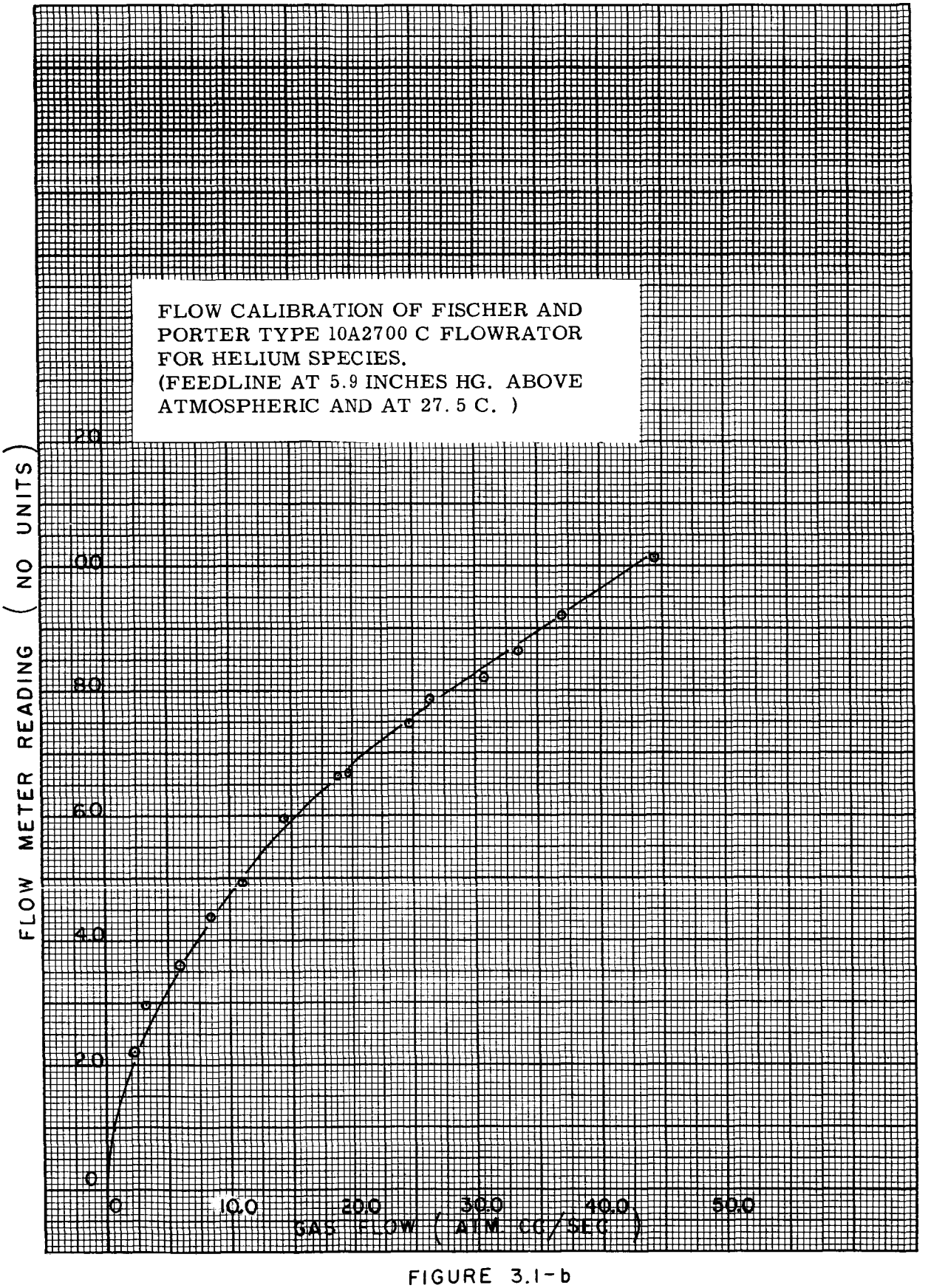
FLOW CALIBRATION OF FISCHER AND PORTER TYPE 10A2700 C FLOWRATOR FOR HELIUM SPECIES.
(FEEDLINE AT 5.9 INCHES HG. ABOVE ATMOSPHERIC AND AT 27.5 C. )
FLOW METER READING ( NO UNITS )
100
80
60
40
20
0
0
10.0
20.0
30.0
40.0
50.0
GAS FLOW ( ATM CC/SEC )

FIGURE 3.1-b

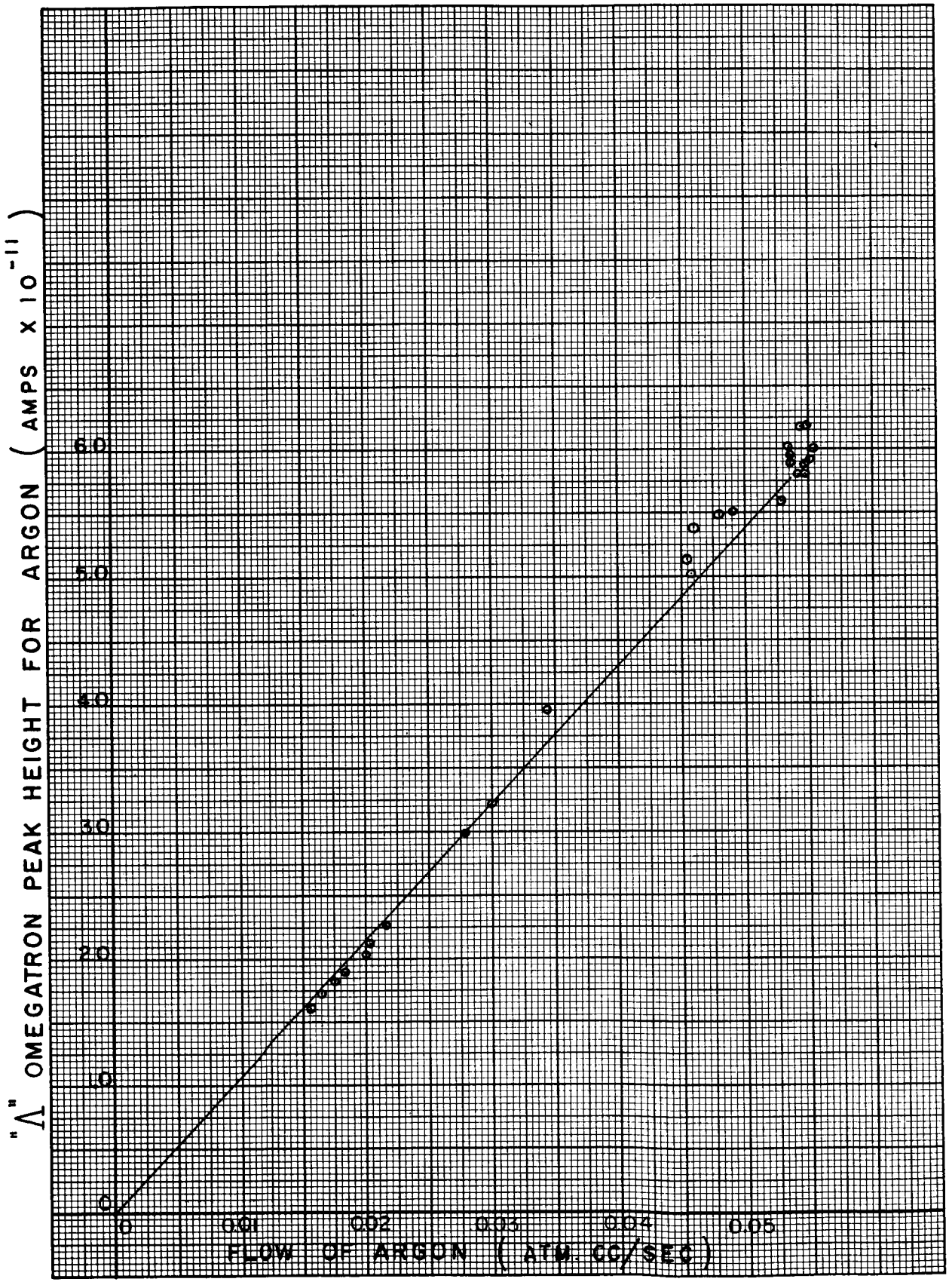
"Λ" OMEGATRON PEAK HEIGHT FOR ARGON ( AMPS X 10⁻¹¹ )
6.0
5.0
4.0
3.0
2.0
1.0
0
0.001
0.002
0.003
0.004
0.005
FLOW OF ARGON ( ATM. CC/SEC )

FIGURE 3.2 - a

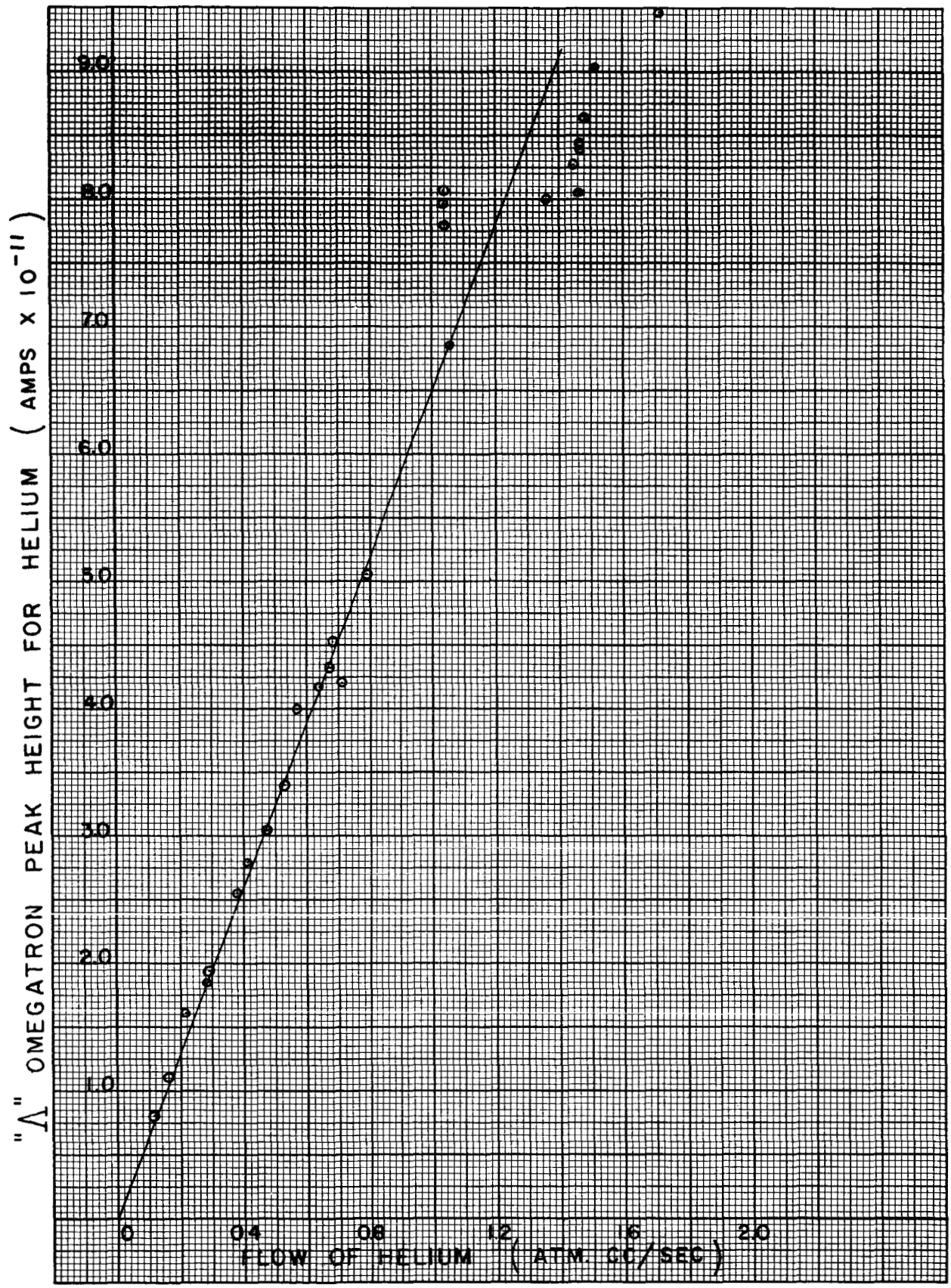
"Λ" OMEGATRON PEAK HEIGHT FOR HELIUM (AMPS X 10⁻¹¹)
9.0
8.0
7.0
6.0
5.0
4.0
3.0
2.0
1.0
0
.04
.08
.12
.16
2.0
FLOW OF HELIUM (ATM. CC/SEC)

FIGURE 3.2-b

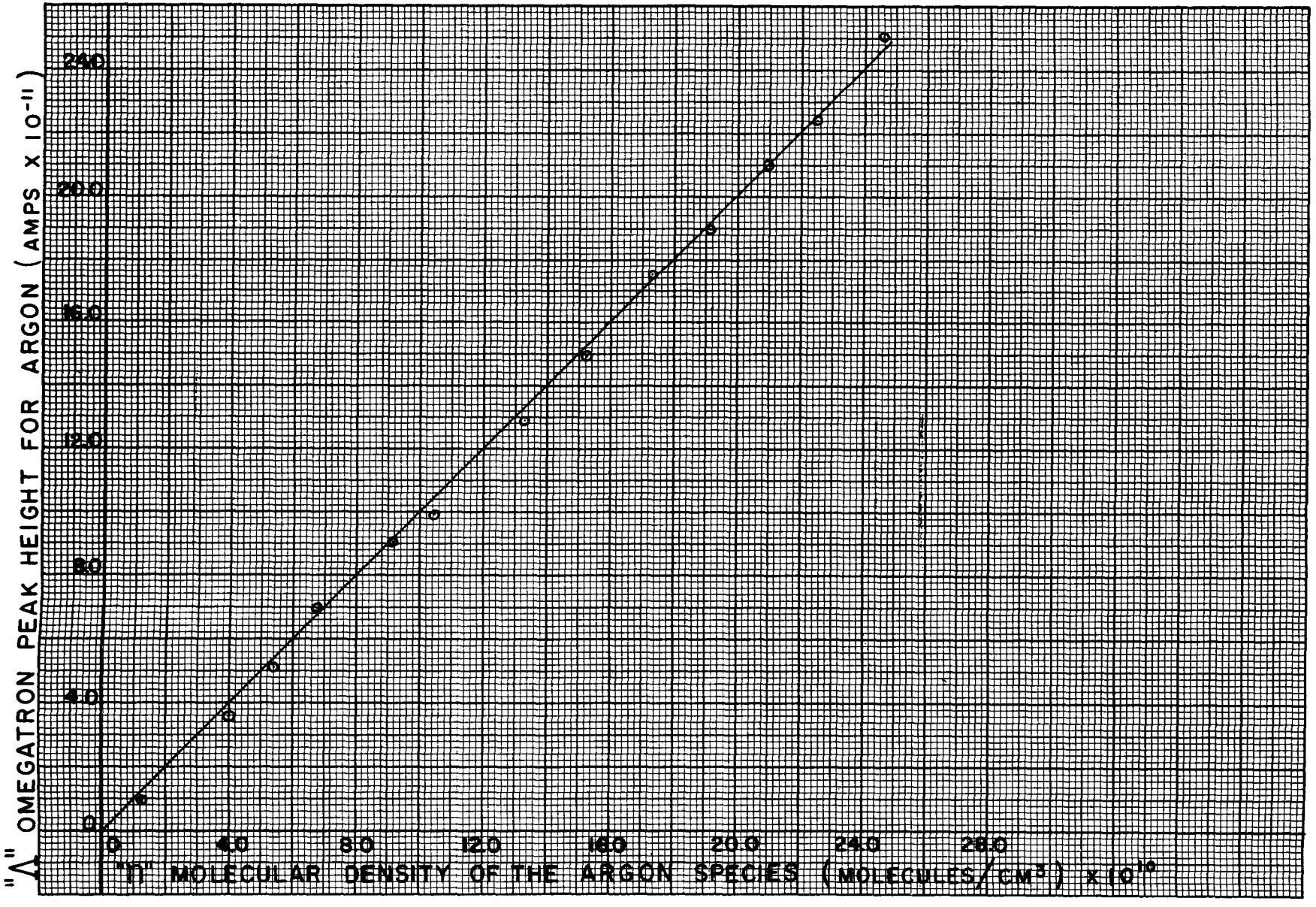
"Δ" OMEGATRON PEAK HEIGHT FOR ARGON (AMPS X 10⁻¹¹)
240
200
160
120
80
40
0
0
40
80
120
160
200
240
280
"n" MOLECULAR DENSITY OF THE ARGON SPECIES (MOLECULES/CM³) X 10¹⁰

FIGURE 3.3-a

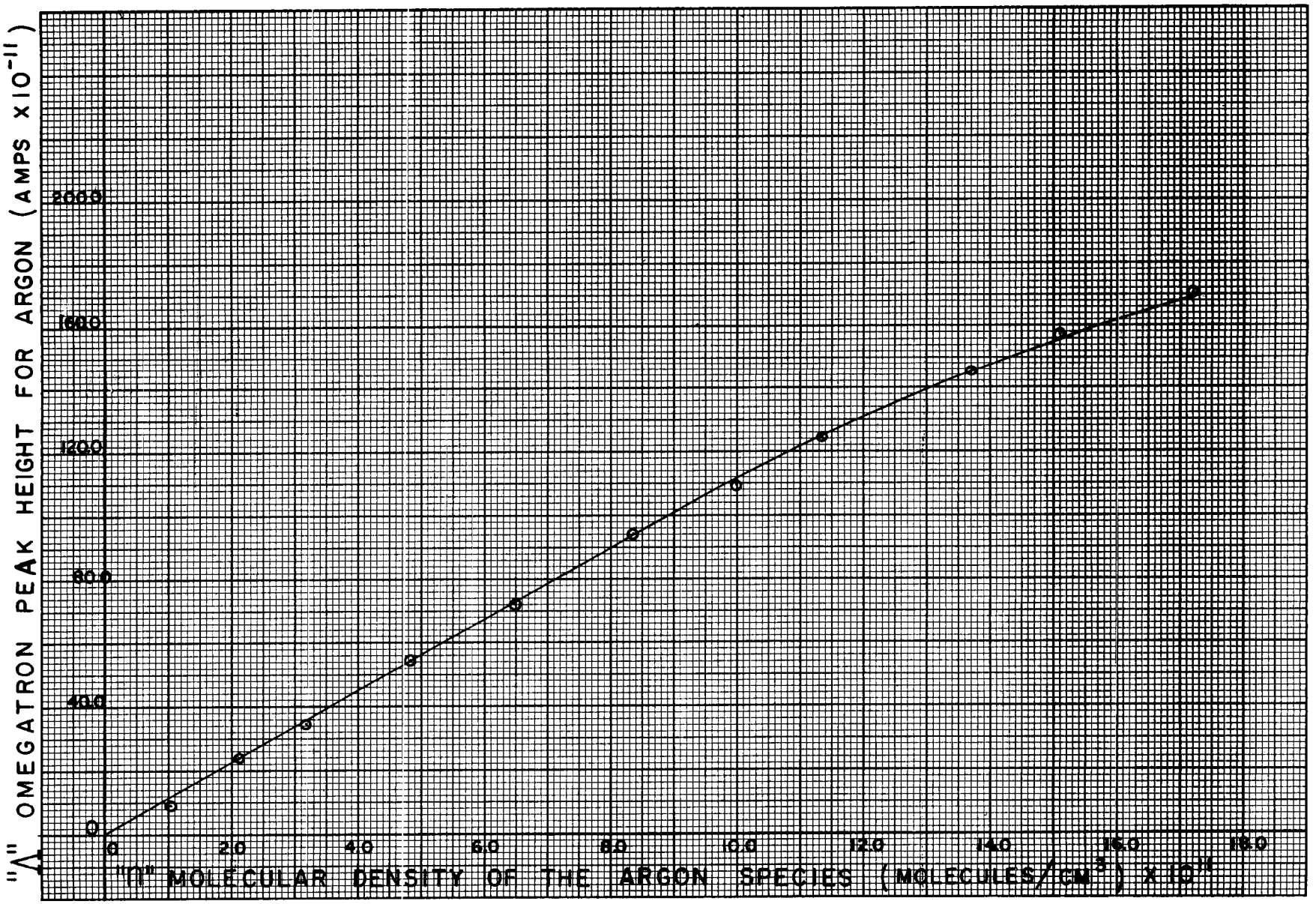
"A" OMEGATRON PEAK HEIGHT FOR ARGON (AMPS X10⁻¹¹)
2000
1600
1200
800
400
0
0
2.0
4.0
6.0
8.0
10.0
12.0
14.0
16.0
18.0
"n" MOLECULAR DENSITY OF THE ARGON SPECIES (MOLECULES/CM³) X 10¹⁴

FIGURE 3.3-b

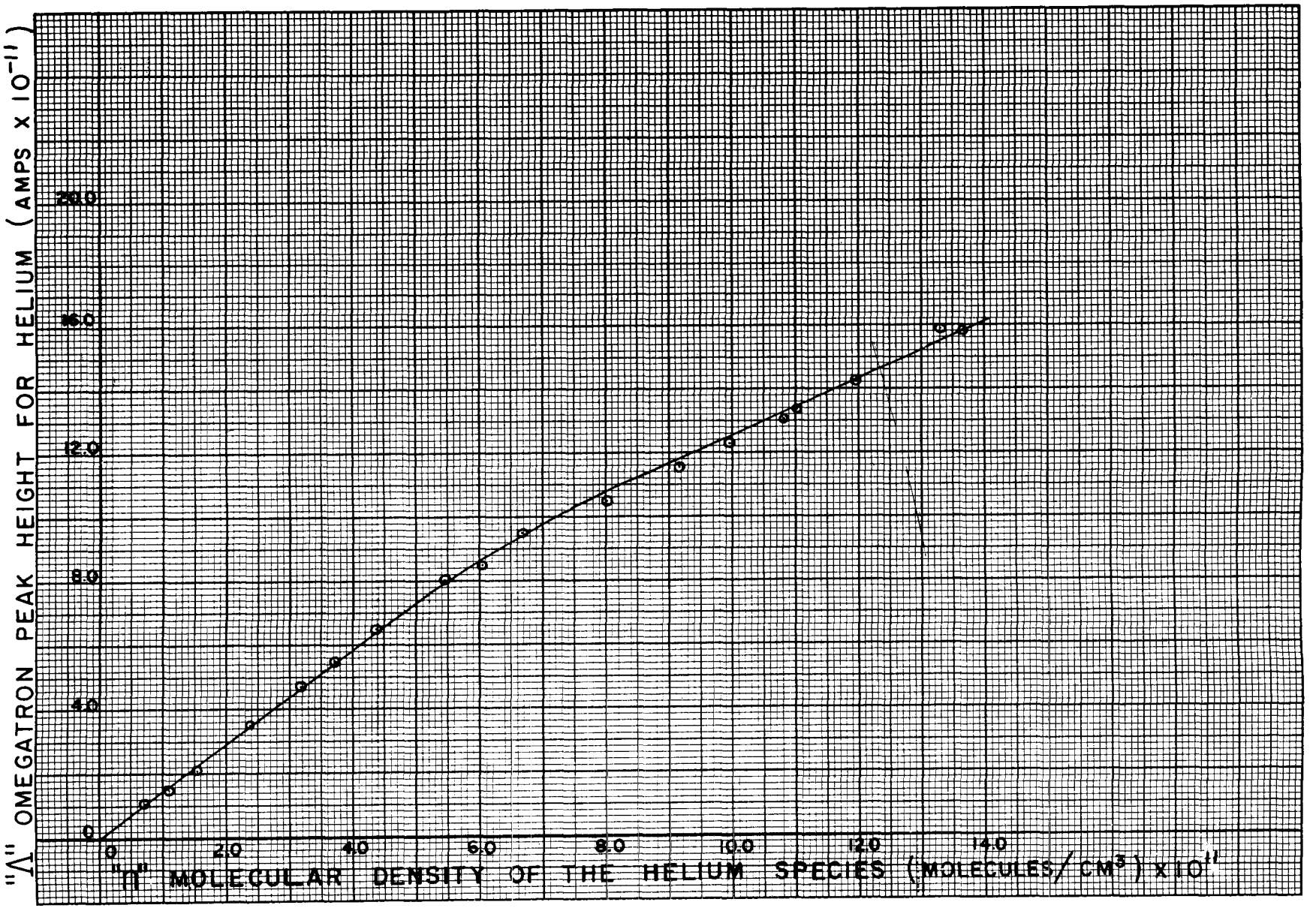
"Λ" OMEGATRON PEAK HEIGHT FOR HELIUM (AMPS x 10⁻¹¹)
20.0
16.0
12.0
8.0
4.0
0
0
2.0
4.0
6.0
8.0
10.0
12.0
14.0
"n" MOLECULAR DENSITY OF THE HELIUM SPECIES (MOLECULES/CM³) x 10¹¹

FIGURE 3.3-c

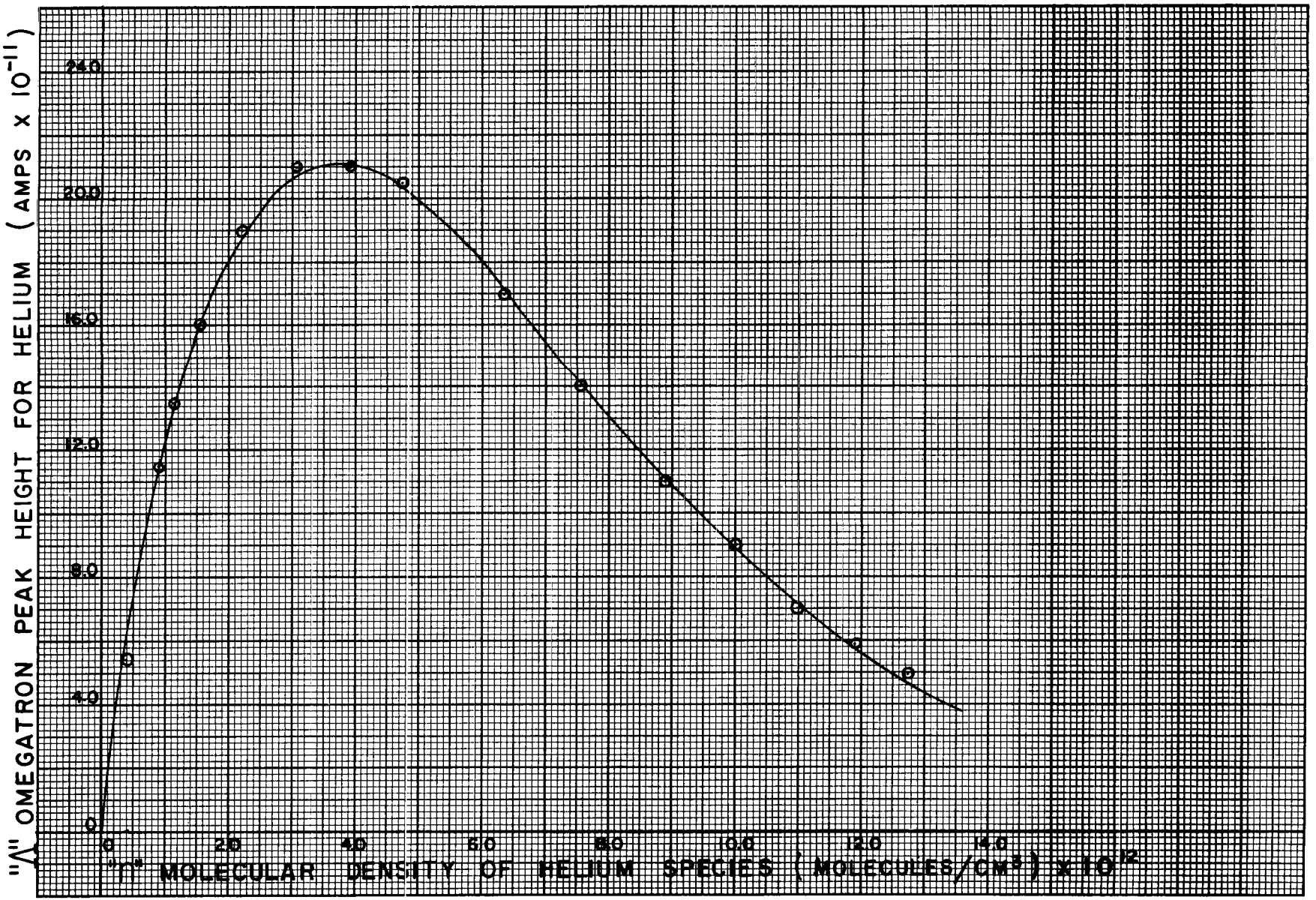
"Δ" OMEGATRON PEAK HEIGHT FOR HELIUM (AMPS X $10^{-11}$)
24.0
20.0
16.0
12.0
8.0
4.0
0
0
2.0
4.0
6.0
8.0
10.0
12.0
14.0
"n" MOLECULAR DENSITY OF HELIUM SPECIES (MOLECULES/$CM^3$) X $10^{12}$

FIGURE 3.3-d

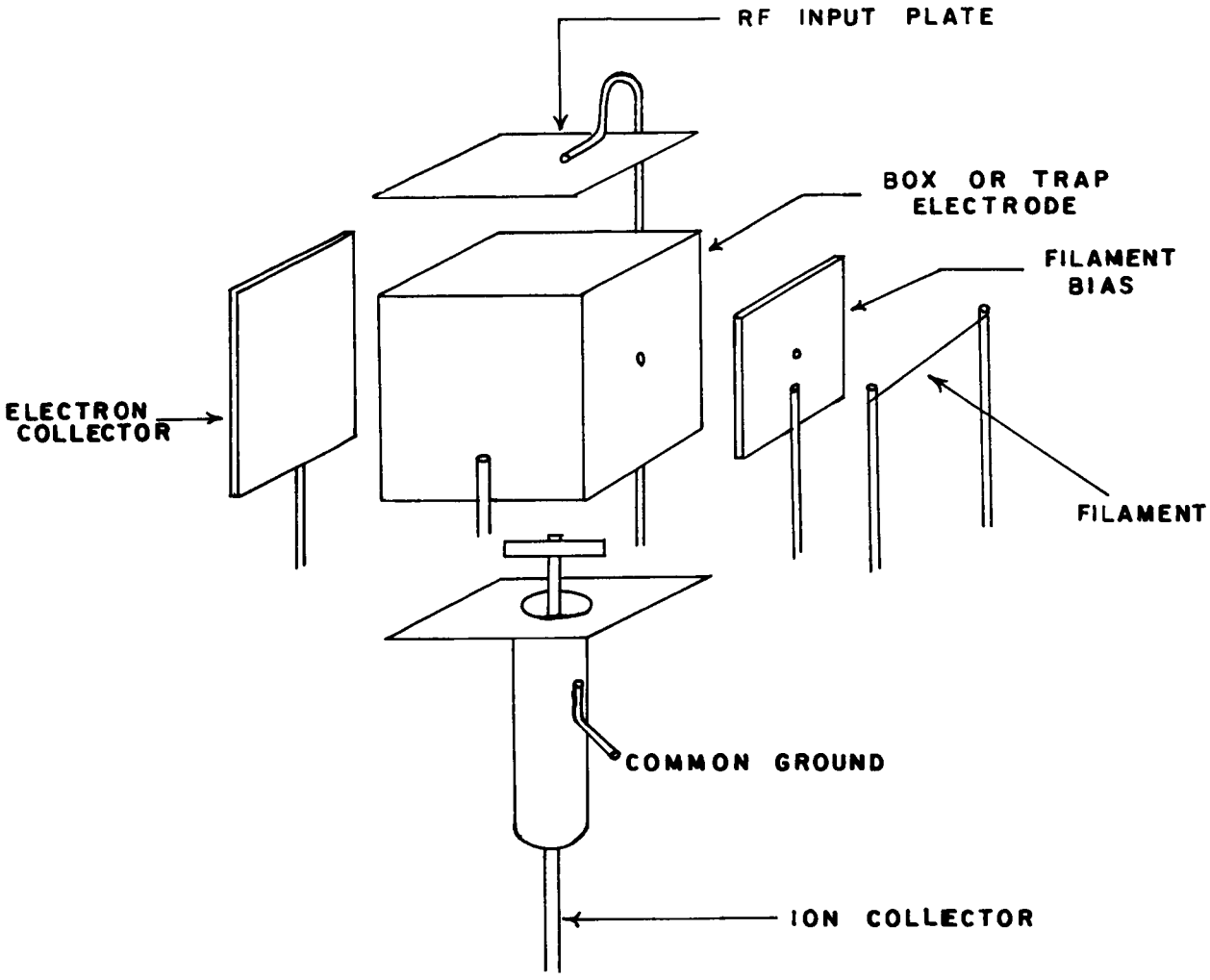


SCHEMATIC OF OMEGATRON ELECTRODE SYSTEM

FIGURE 3.3-e

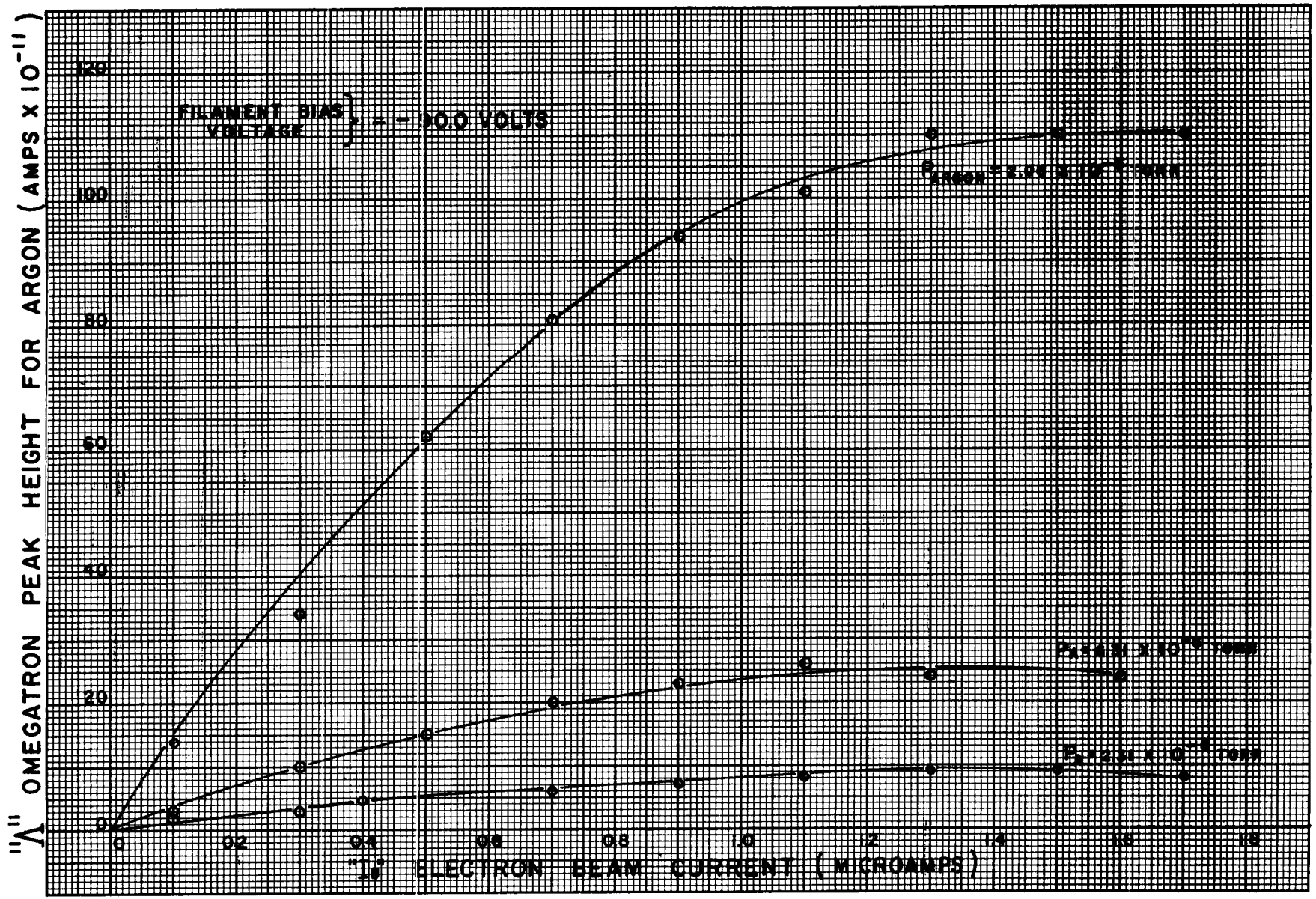
"I" OMEGATRON PEAK HEIGHT FOR ARGON (AMPS X 10⁻¹¹)
FILAMENT BIAS VOLTAGE } = −100 VOLTS
P_ARGON = 2.94 X 10⁻⁶ TORR
P = 4.91 X 10⁻⁶ TORR
P = 2.94 X 10⁻⁶ TORR
"I" ELECTRON BEAM CURRENT (MICROAMPS)
0
20
40
60
80
100
120
.02
.04
.06
.08
.10
.12
.14
.16
.18

FIGURE 3.3-f

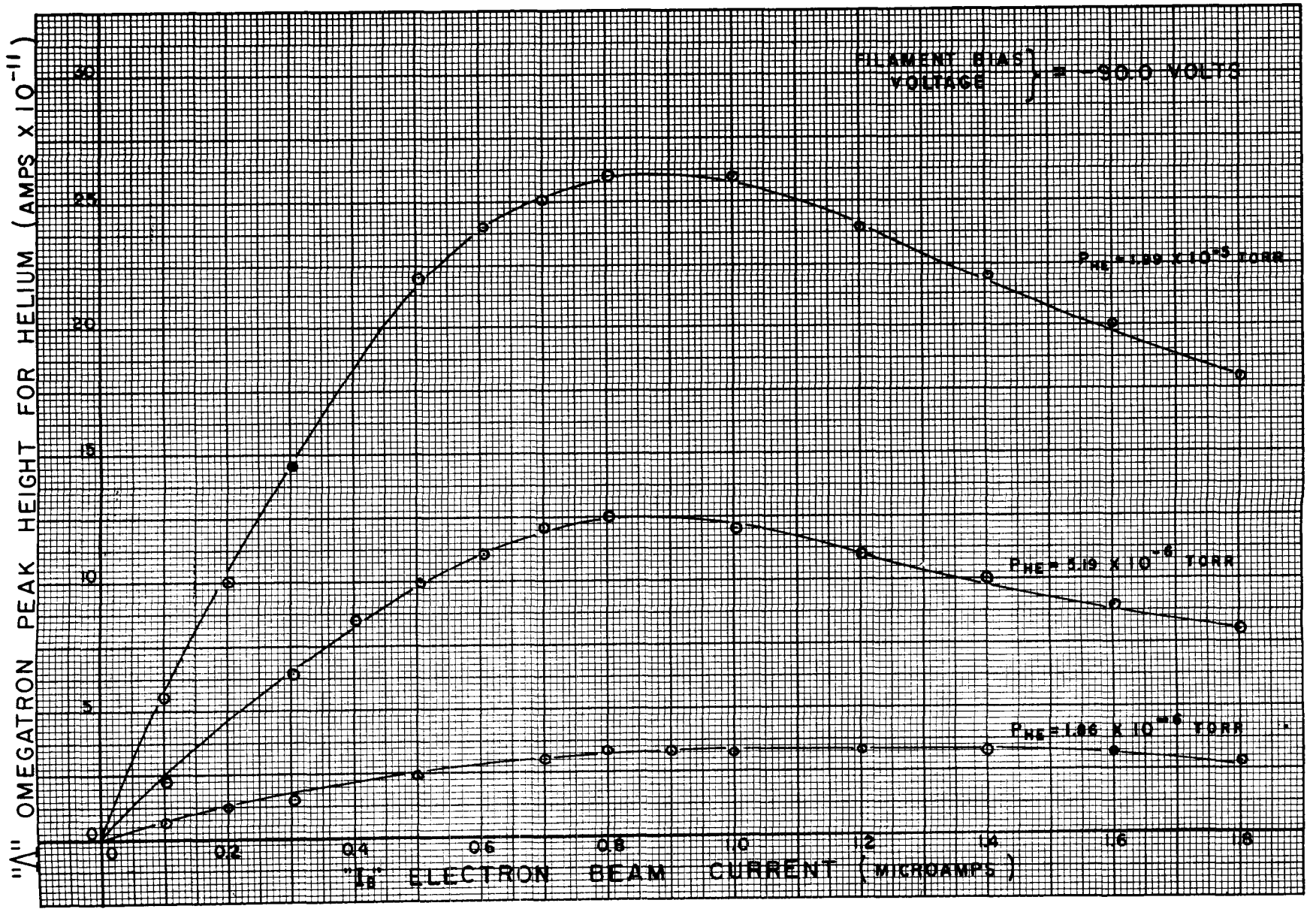
FILAMENT BIAS VOLTAGE = −90.0 VOLTS
$P_{HE}$ = 5.29 X 10⁻⁵ TORR
$P_{HE}$ = 5.19 X 10⁻⁶ TORR
$P_{HE}$ = 1.06 X 10⁻⁶ TORR
"A" OMEGATRON PEAK HEIGHT FOR HELIUM (AMPS X 10⁻¹¹)
"$I_E$" ELECTRON BEAM CURRENT (MICROAMPS)
0
5
10
15
20
25
30
0.2
0.4
0.6
0.8
1.0
1.2
1.4
1.6
1.8

FIGURE 3.3-9

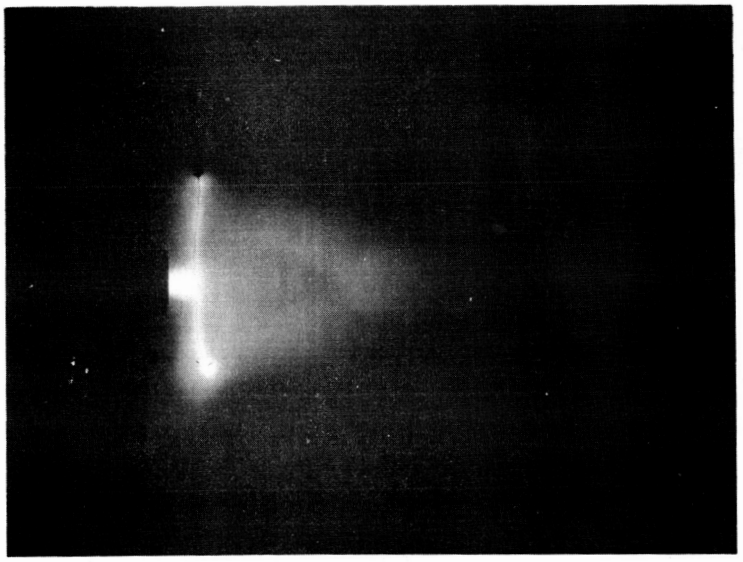

FIGURE 3.4- a FREE JET EXPANSION, NOZZLE DIAMETER= 2", PRESSURE 299 MICRONS, STATIC PRESSURE 19 MICRONS.

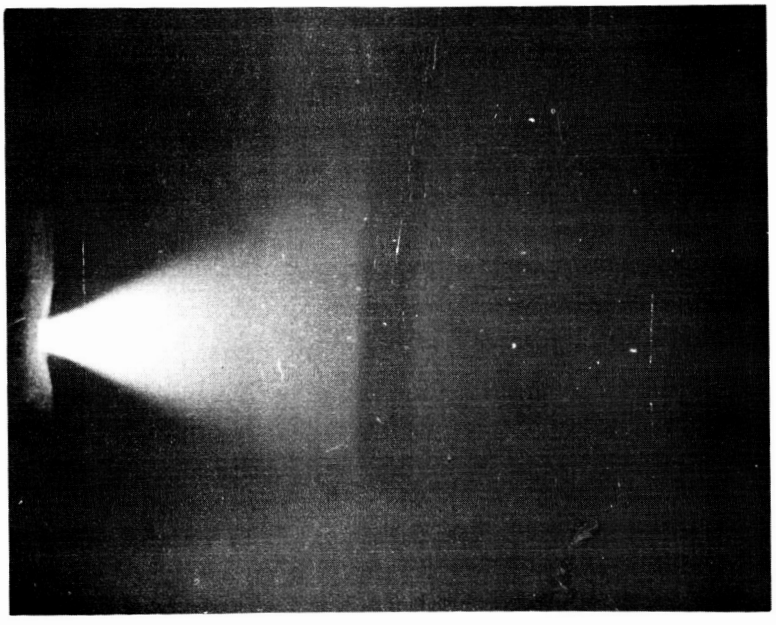

FIGURE 3.4- b FREE JET, NOZZLE DIAMETER = 0.031", STAGNATION PRESSURE 100 MM HG, STATIC PRESSURE 25 MICRONS.

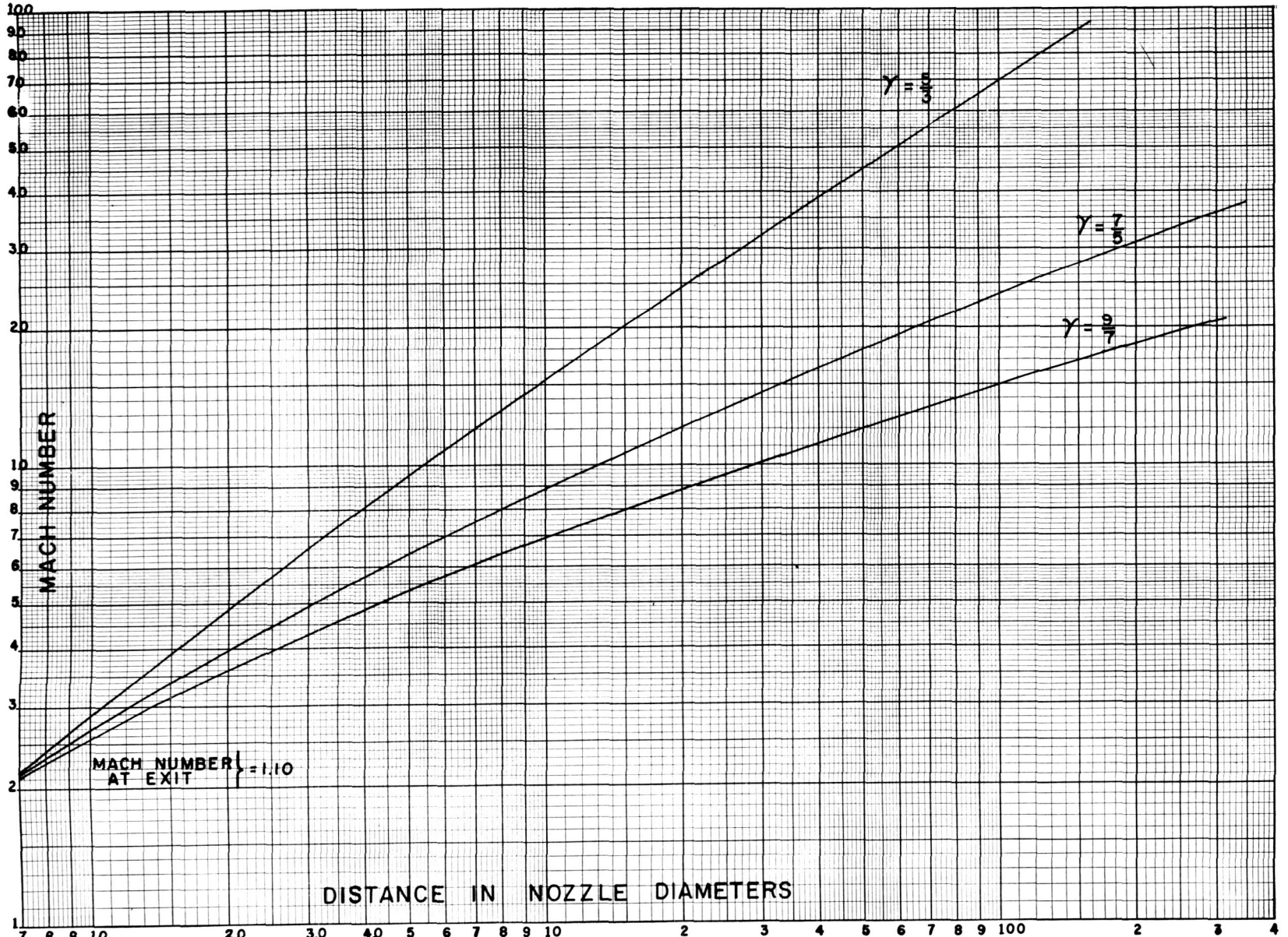
MACH NUMBER
DISTANCE IN NOZZLE DIAMETERS
$\gamma = \frac{5}{3}$
$\gamma = \frac{7}{5}$
$\gamma = \frac{9}{7}$
MACH NUMBER AT EXIT = 1.10
100
90
80
70
60
50
40
30
20
10
9
8
7
6
5
4
3
2
1
.7 .8 .9 1.0 2.0 3.0 4.0 5 6 7 8 9 10 2 3 4 5 6 7 8 9 100 2 3 4

FIGURE 3.4-c

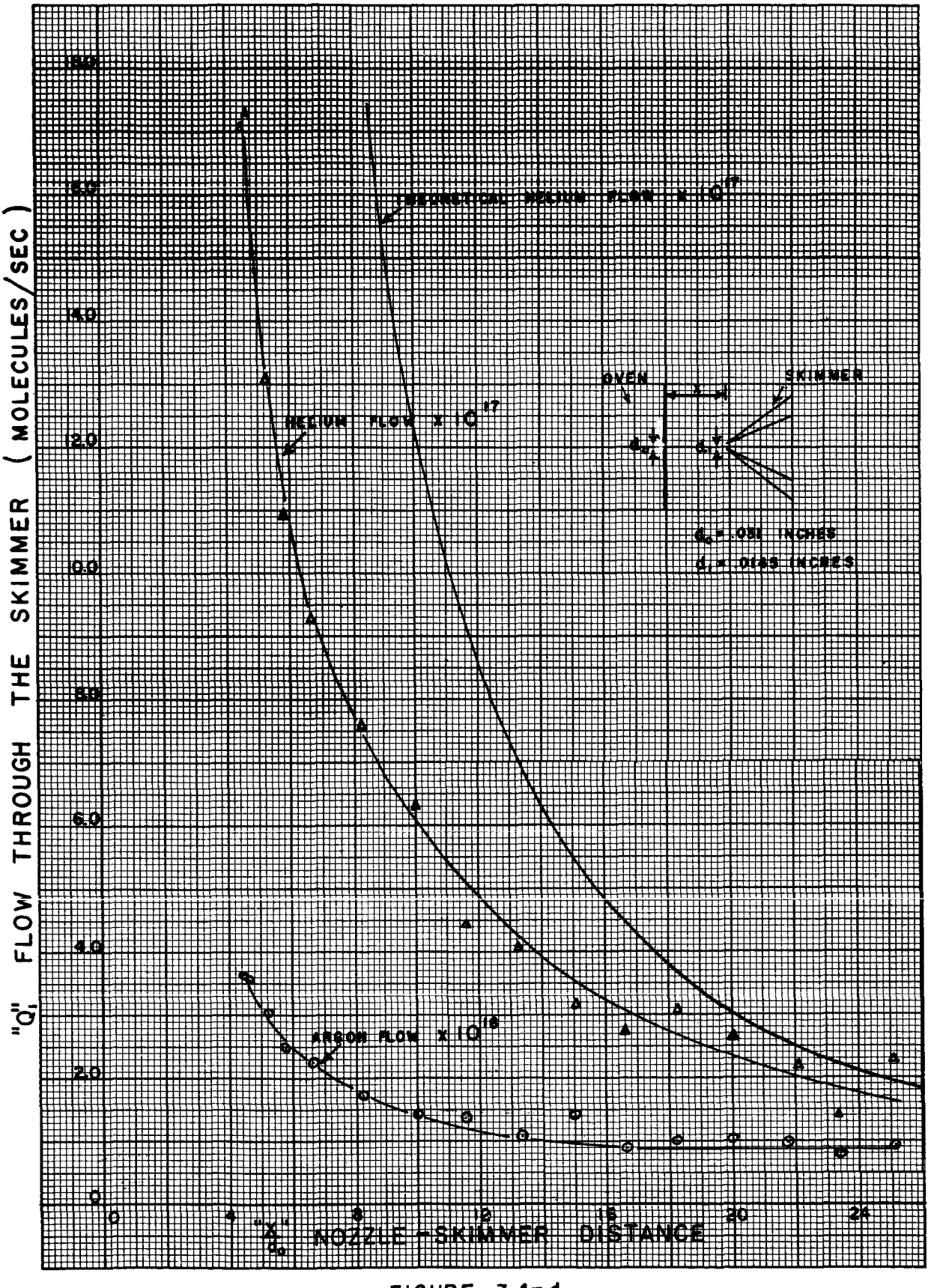
"Q" FLOW THROUGH THE SKIMMER ( MOLECULES/SEC )
16.0
14.0
12.0
10.0
8.0
6.0
4.0
2.0
0
0
4
8
12
15
20
24
"X" NOZZLE - SKIMMER DISTANCE
THEORETICAL HELIUM FLOW x 10^17
HELIUM FLOW x 10^17
ARGON FLOW x 10^16
OVEN
SKIMMER
d0 = .031 INCHES
d1 = .0165 INCHES

FIGURE 3.4-d

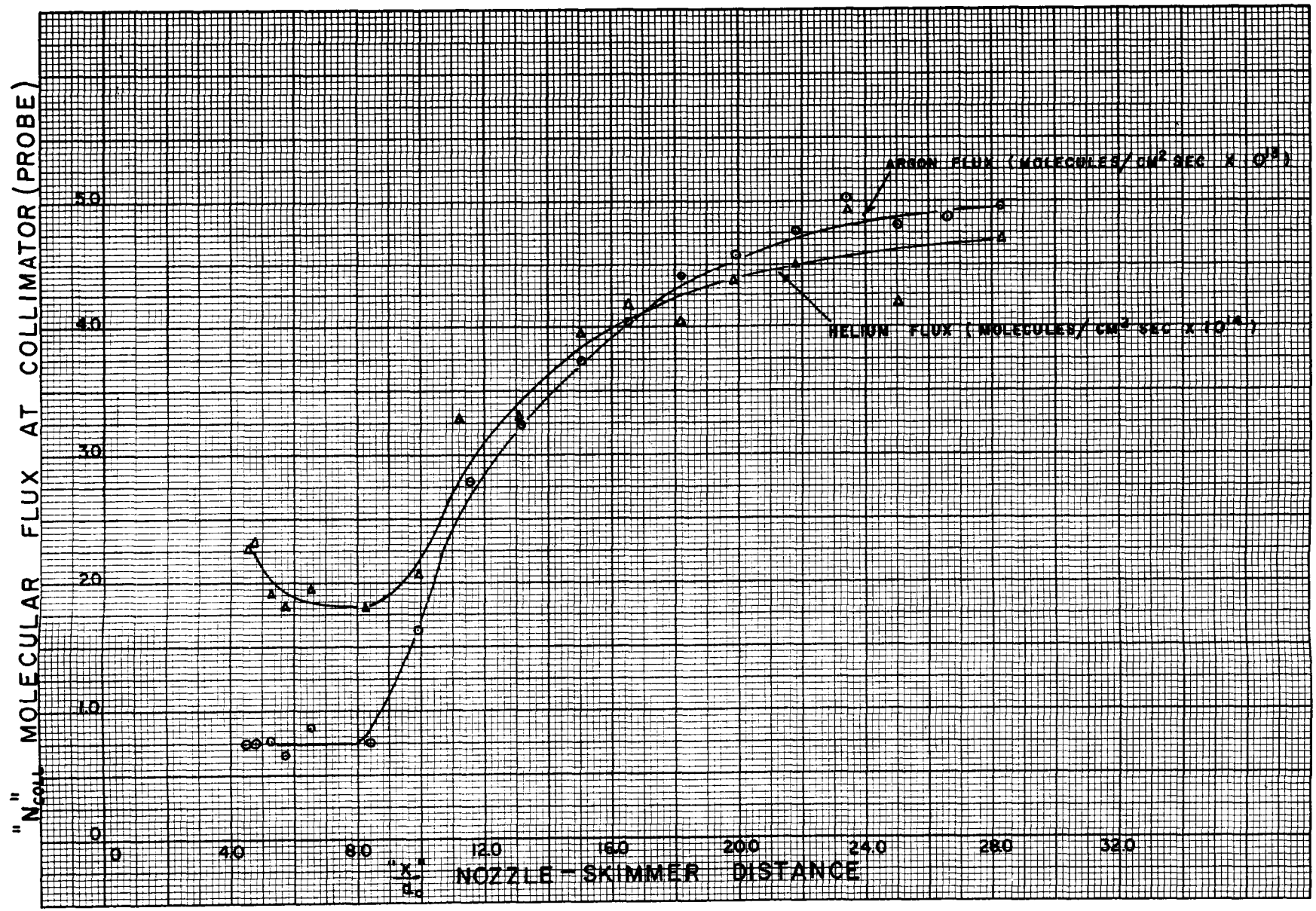
"N_COL" MOLECULAR FLUX AT COLLIMATOR (PROBE)
5.0
4.0
3.0
2.0
1.0
0
0
4.0
8.0
12.0
16.0
20.0
24.0
28.0
32.0
"X/d_o" NOZZLE-SKIMMER DISTANCE
ARGON FLUX (MOLECULES/CM² SEC X 10¹⁵)
HELIUM FLUX (MOLECULES/CM² SEC X 10¹⁶)

FIGURE 3.6-a

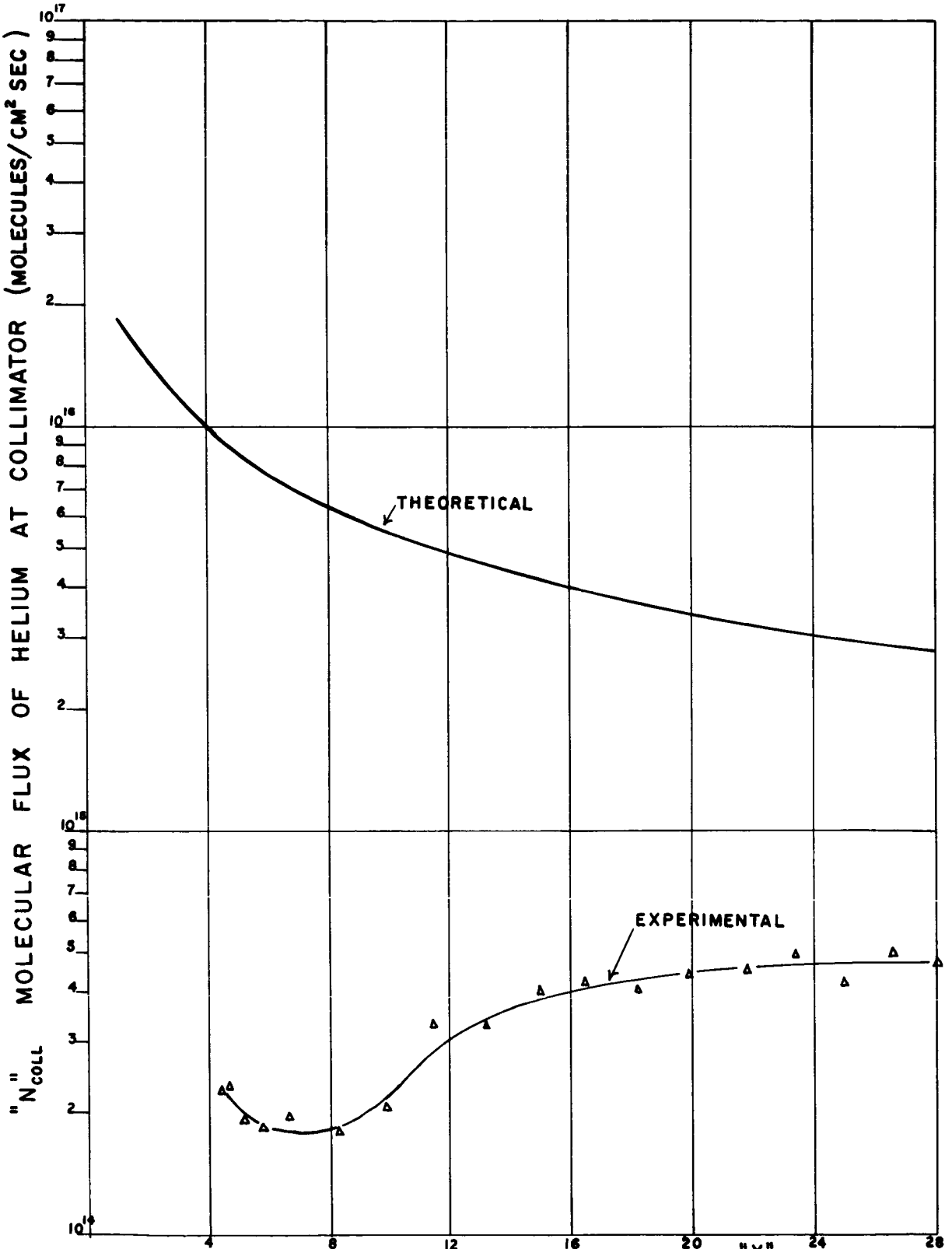
"N_COLL" MOLECULAR FLUX OF HELIUM AT COLLIMATOR (MOLECULES/CM² SEC)
10¹⁷
10¹⁶
10¹⁵
THEORETICAL
EXPERIMENTAL
4
8
12
16
20
24
28
"X"/d_o NOZZLE - SKIMMER DISTANCE

FIGURE 3.6-b

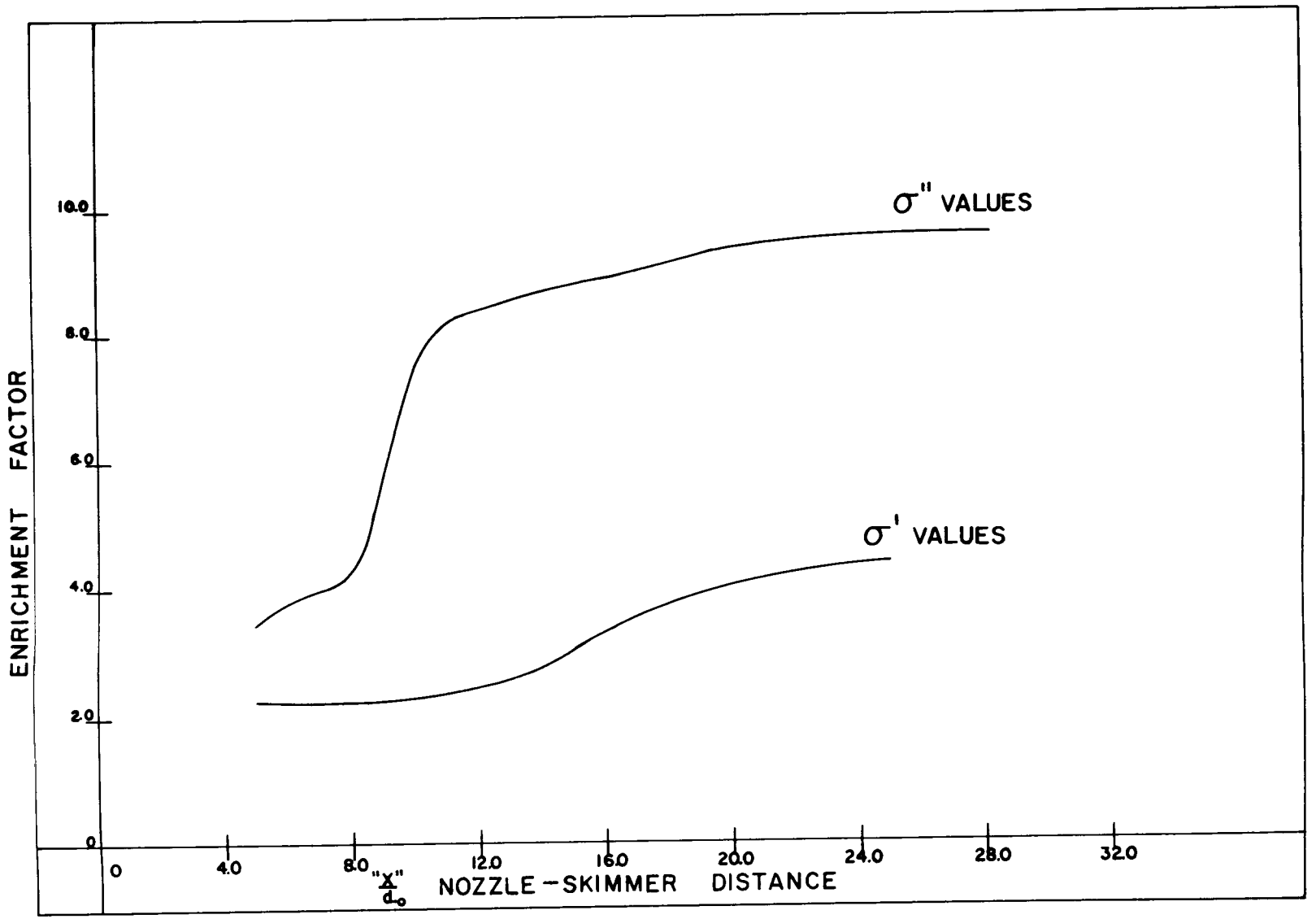
ENRICHMENT FACTOR
10.0
8.0
6.0
4.0
2.0
0
σ'' VALUES
σ' VALUES
0
4.0
8.0
12.0
16.0
20.0
24.0
28.0
32.0
"X"/d₀
NOZZLE – SKIMMER DISTANCE

FIGURE 3.6-c

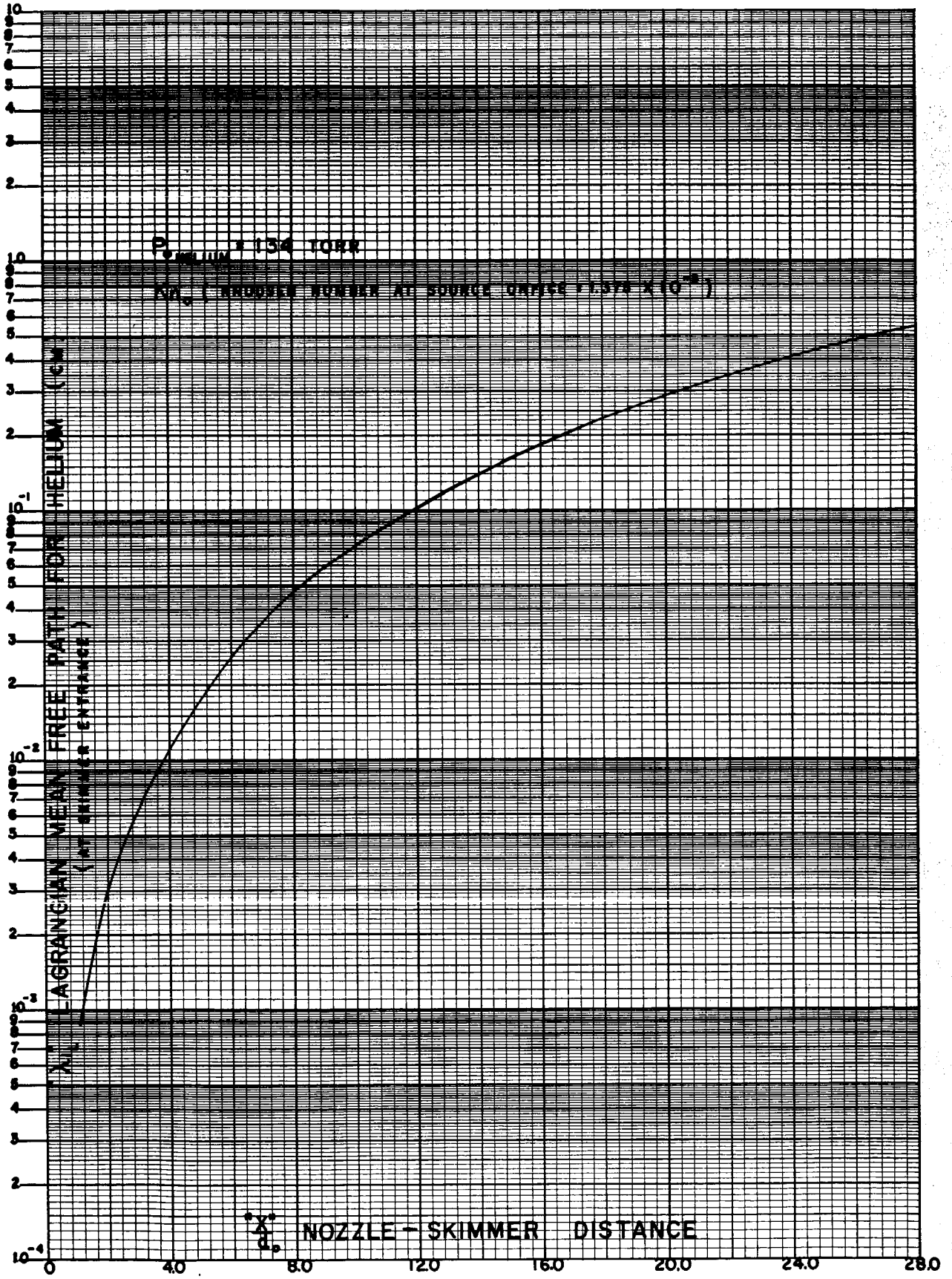
$P_{HELIUM}$ = 134 TORR
$Kn_D$ ( KNUDSEN NUMBER AT SOURCE ORIFICE = 1.574 x $10^{-3}$ )
LAGRANGIAN MEAN FREE PATH FOR HELIUM (CM)
( at stagnation entrance )
$\frac{X}{d_p}$ NOZZLE - SKIMMER DISTANCE
0
4.0
8.0
12.0
16.0
20.0
24.0
28.0

FIGURE 3.6 - d

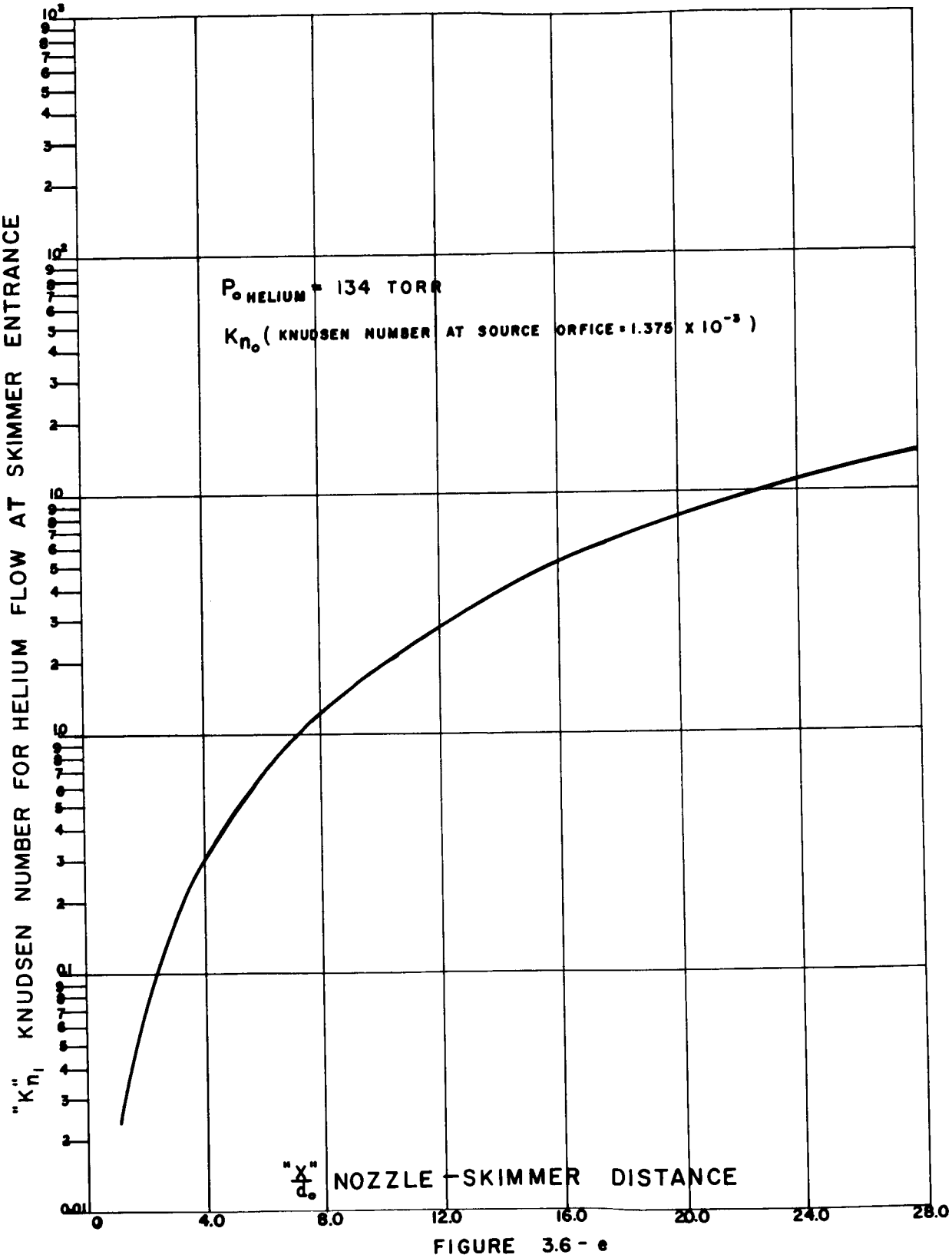
"$K_{n_1}$" KNUDSEN NUMBER FOR HELIUM FLOW AT SKIMMER ENTRANCE
$P_{o\,HELIUM}$ = 134 TORR
$K_{n_o}$ ( KNUDSEN NUMBER AT SOURCE ORFICE = 1.375 X $10^{-3}$ )
"$\frac{X}{d_o}$" NOZZLE - SKIMMER DISTANCE
0
4.0
8.0
12.0
16.0
20.0
24.0
28.0

FIGURE 3.6 - e

FIGURE 3.7 - a

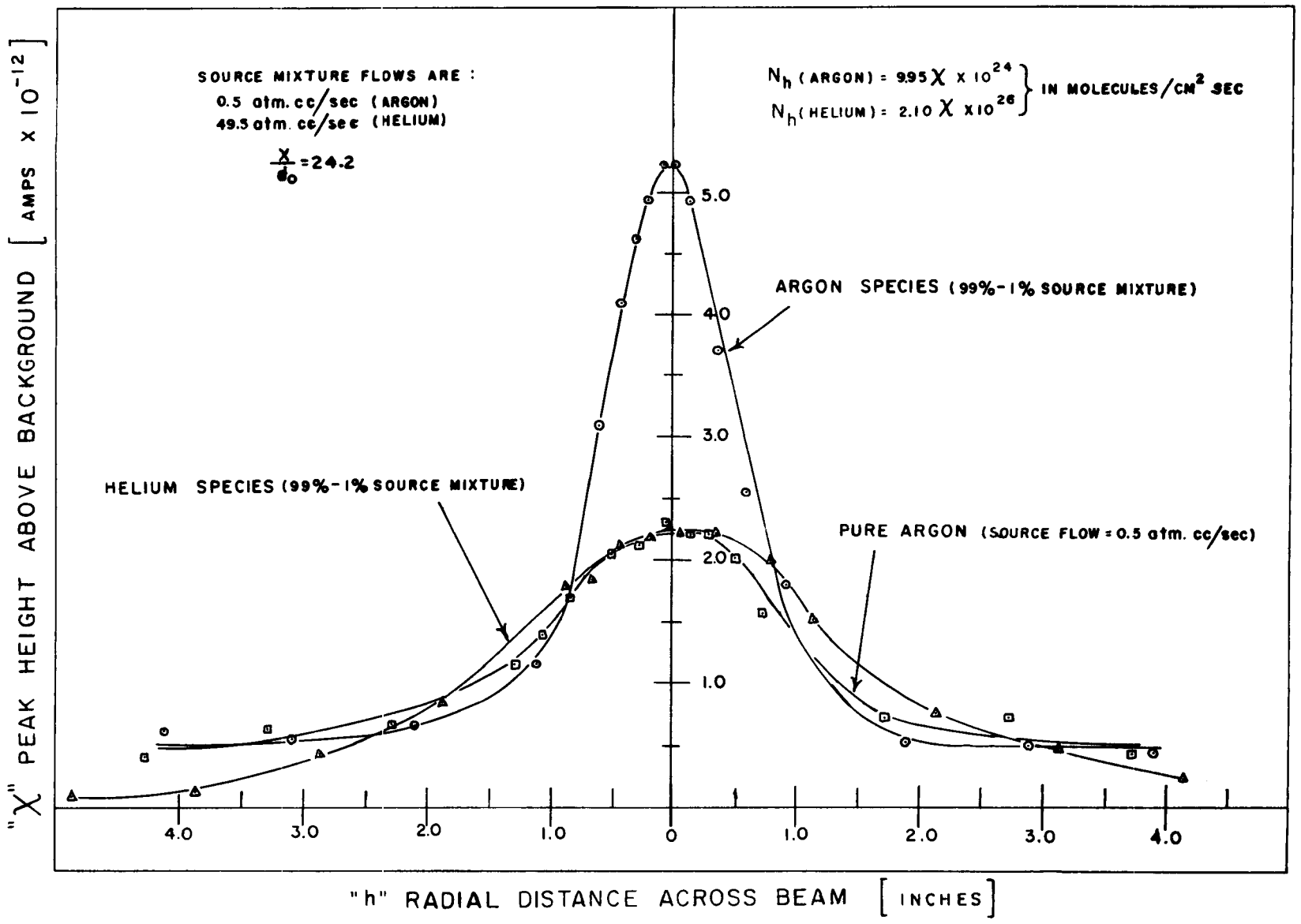


RADIAL FLUX DISTRIBUTION OF THE GAS SPECIES IN THE COLLIMATION CHAMBER

FIGURE 3.7 - b

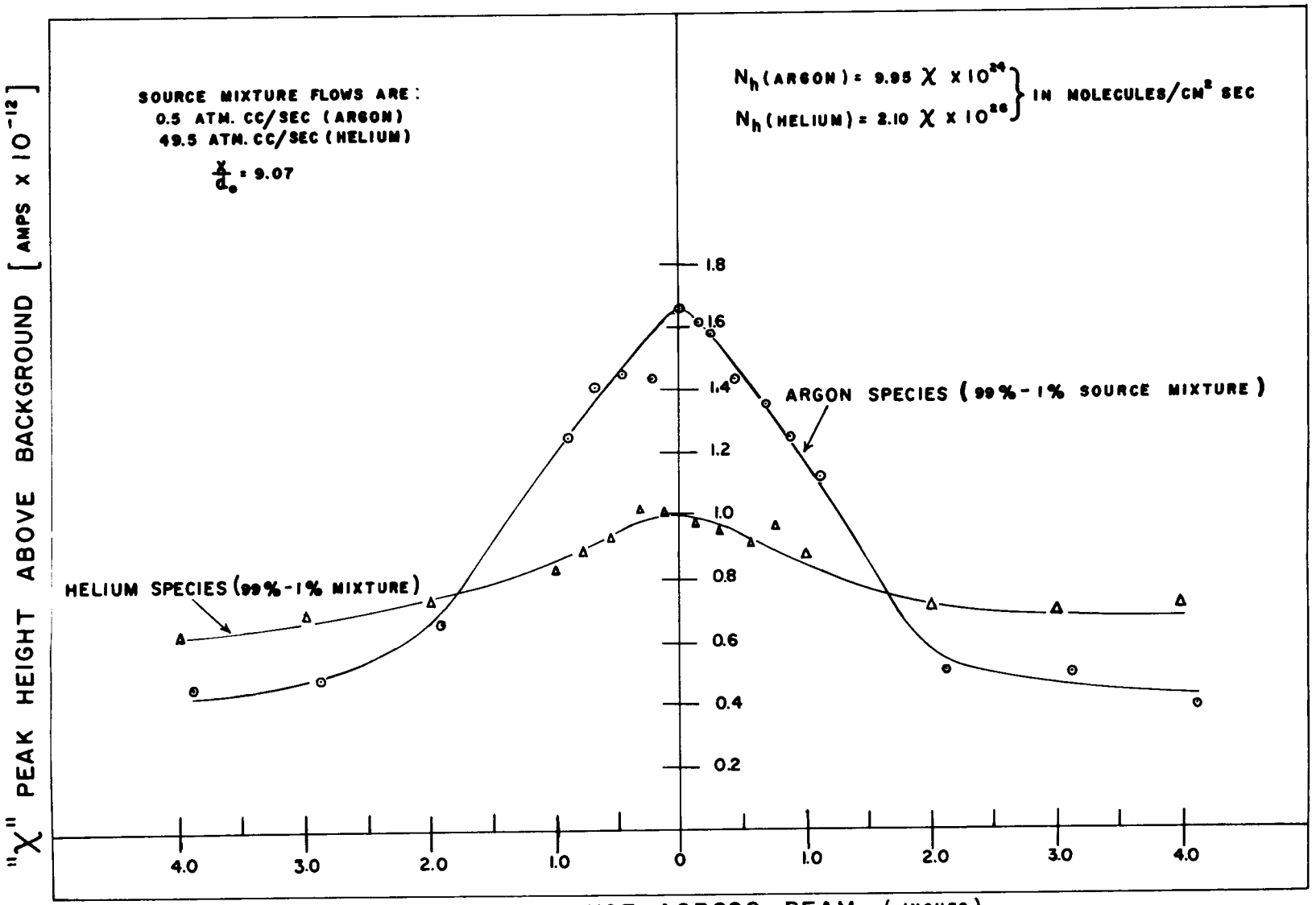


RADIAL FLUX DISTRIBUTION OF THE GAS SPECIES IN THE COLLIMATION CHAMBER

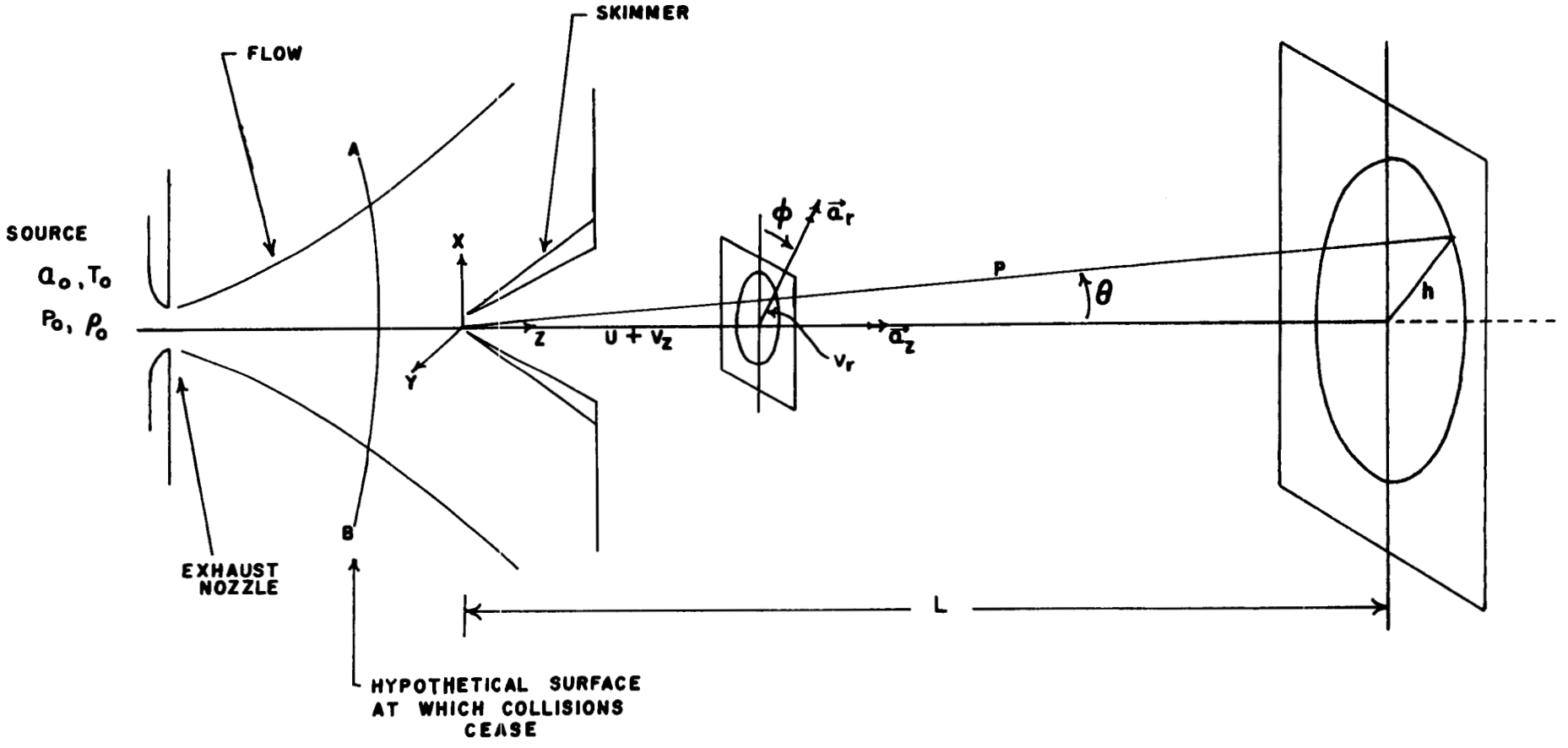
SKIMMER
FLOW
A
SOURCE
$a_o, T_o$
$P_o, \rho_o$
X
Y
Z
$U + V_z$
$\phi$
$\vec{a}_r$
$V_r$
$\vec{a}_z$
P
$\theta$
h
B
EXHAUST NOZZLE
L
HYPOTHETICAL SURFACE AT WHICH COLLISIONS CEASE

FIGURE 3.9-a

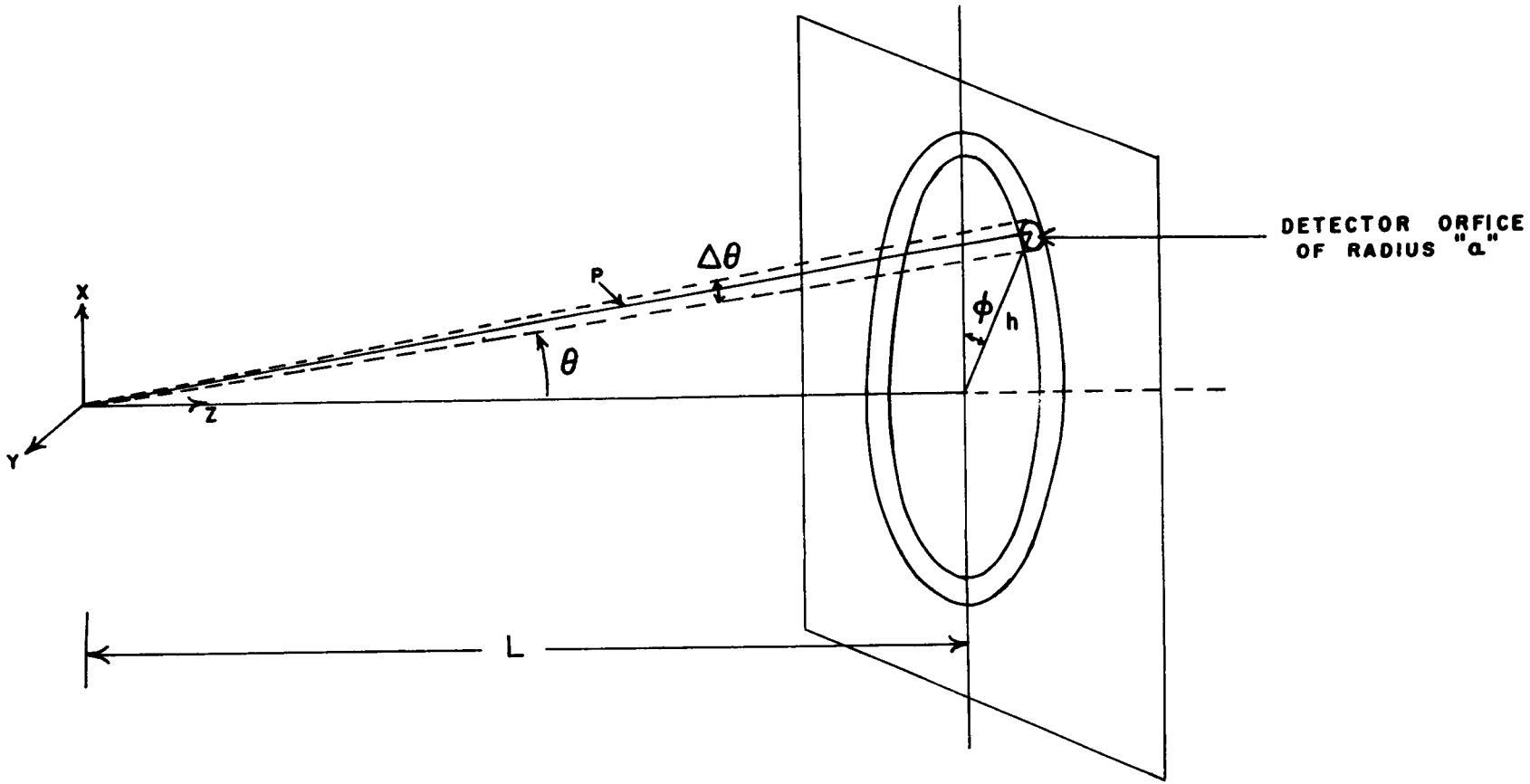


FIGURE 3.9 – b

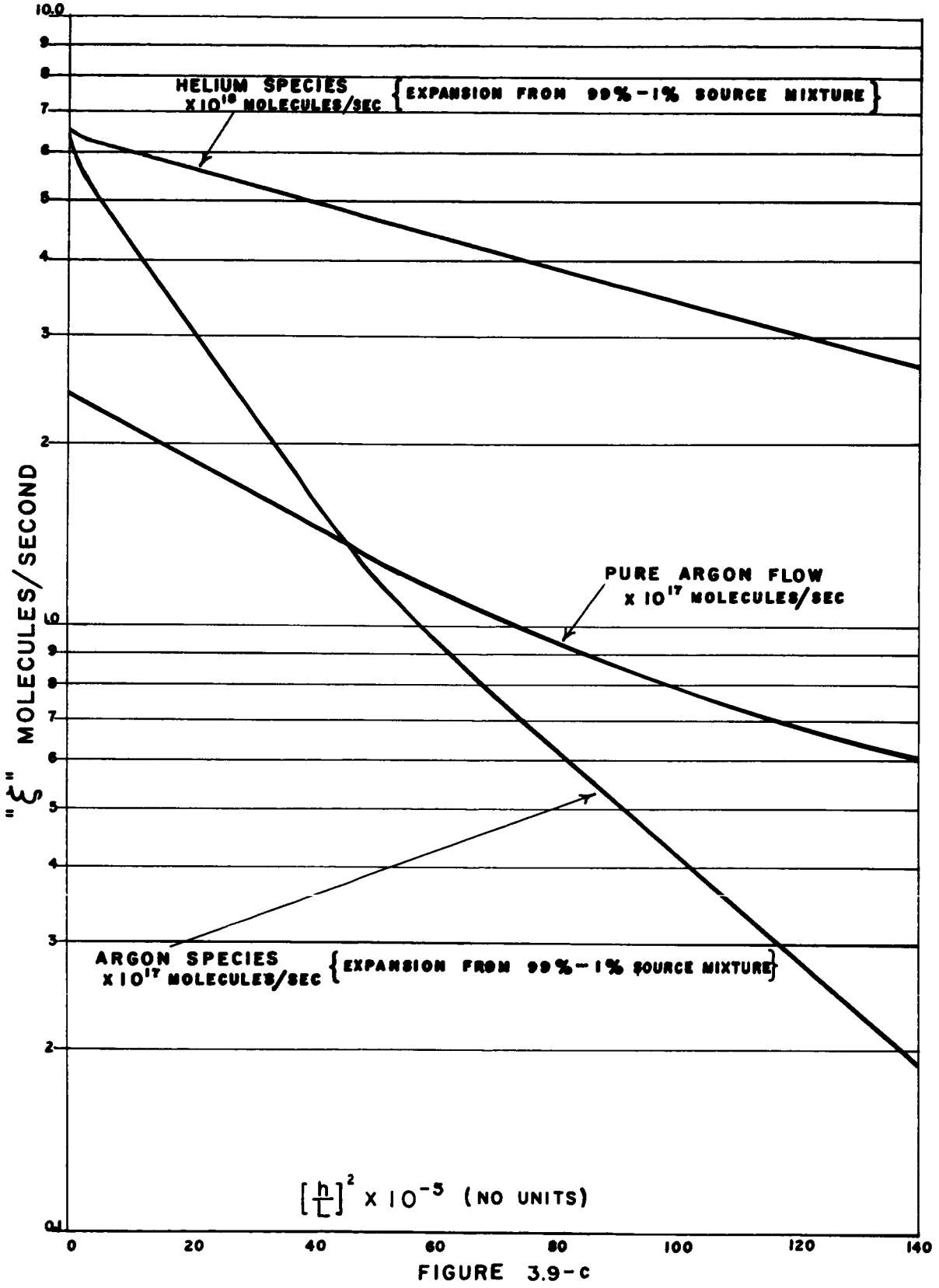
HELIUM SPECIES
X 10^18 MOLECULES/SEC
{EXPANSION FROM 99% - 1% SOURCE MIXTURE}
PURE ARGON FLOW
X 10^17 MOLECULES/SEC
ARGON SPECIES
X 10^17 MOLECULES/SEC
{EXPANSION FROM 99% - 1% SOURCE MIXTURE}
"ξ" MOLECULES/SECOND
[h/L]^2 X 10^-5 (NO UNITS)
10.0
9
8
7
6
5
4
3
2
6
9
8
7
6
5
4
3
2
0.1
0
20
40
60
80
100
120
140

FIGURE 3.9-c

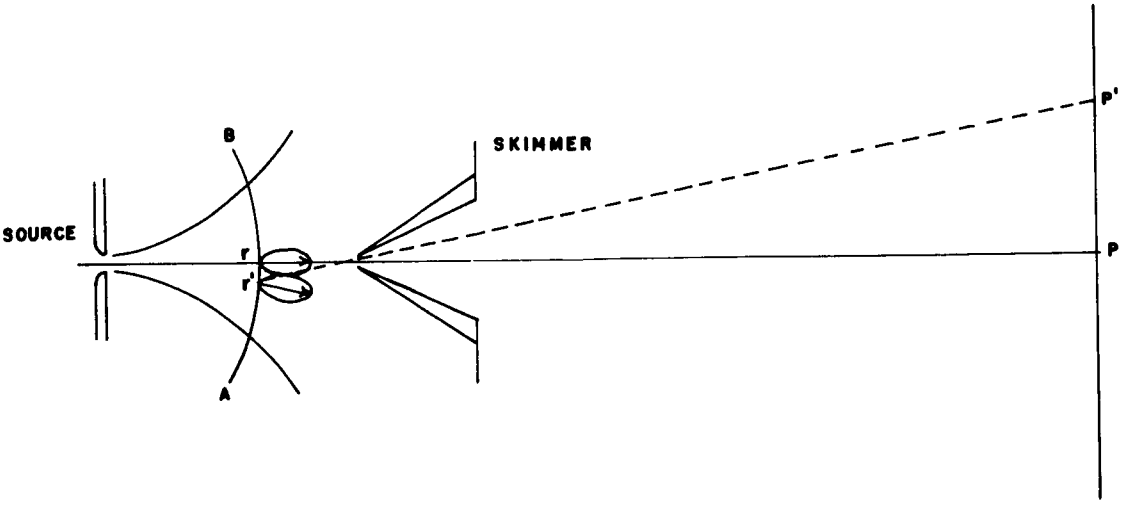


FIGURE 3.9-c

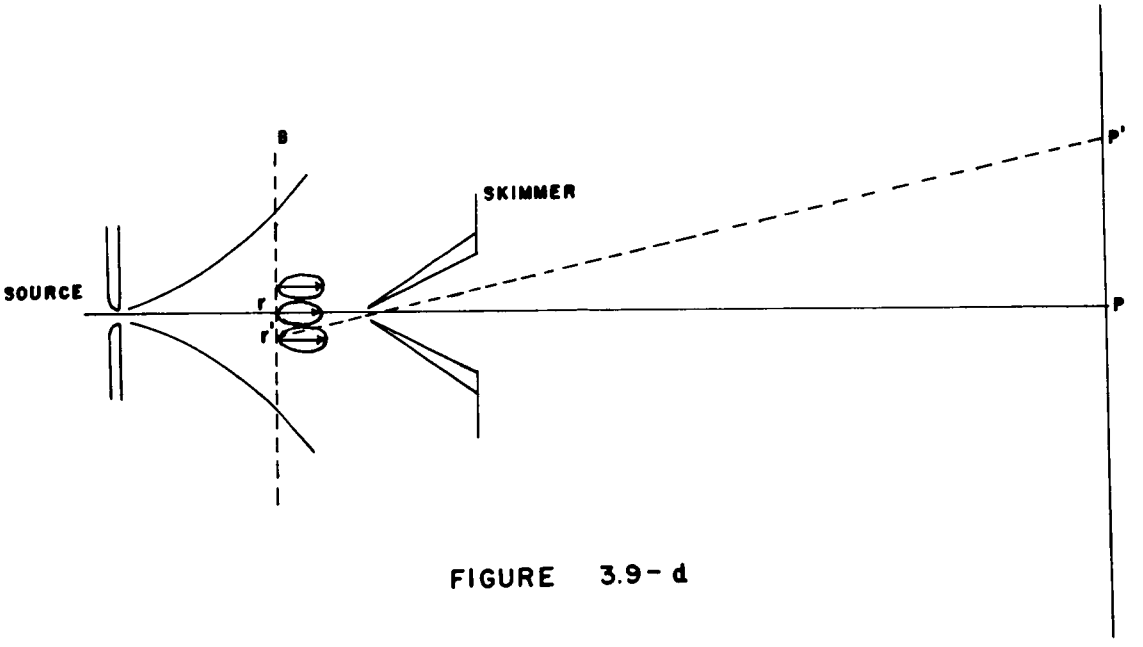


FIGURE 3.9-d